Synchronous Thermal Instability Evaluation of Medium Speed Turbocharger Rotor-Bearing Systems

Brian R. Carroll

Thesis submitted to the faculty of
Virginia Polytechnic Institute and State University
in partial fulfillment of the requirements for the degree

Master of Science
in
Mechanical Engineering

R. Gordon Kirk, Chair
Mary E. Kasarda
Alan A. Kornhauser

May 9, 2012
Blacksburg, Virginia

Keywords: Turbocharger, Rotordynamics, Morton Effect

Abstract

Synchronous Thermal Instability Evaluation of
Medium Speed Turbocharger Rotor-Bearing Systems

Brian R. Carroll

Rotors in fluid-film bearing supported turbomachinery are known to develop elliptical orbits as a result of rotor-bearing interactions, mass unbalance within the rotor, gravitational bending of the shaft and external excitation. In synchronous whirl, where the speed at which the shaft travels about the orbit is equal to the rotational speed of the rotor, temperature gradients may develop across the journal as a result of viscous shear in the bearing's lubricant film. This thermal gradient leads to bending of the shaft in a phenomenon known as The Morton Effect. Such thermally induced bending causes further growth of the elliptical orbit resulting in further bending leading to excessive vibration levels and premature bearing failure. This analysis examines the development of the Morton Effect in medium-speed turbochargers typical to shipboard propulsion engines and the effect that bearing clearance has on thermal stability. Floating ring and tilting pad journal bearings are considered with a single stage, overhung centrifugal compressor and an overhung axial turbine. Results indicate a correlation between bearing clearance and thermal stability in the rotor-bearing system.

A model for the aerodynamic force generated as a result of interaction between air exiting a centrifugal compressor and the compressor's annulus in a turbocharger is then developed and applied to the rotor-bearing systems. Results suggest little correlation between this aerodynamic force and the development of the Morton Effect.

Acknowledgements

I would like to take a moment to express my gratitude for the support I received during my studies.

First, I would like to thank Dr. Gordon Kirk for the technical guidance and general support he consistently provided during my time at Virginia Tech. I truly appreciate the space he gave me to work and learn while remaining available whenever I needed assistance. His help was instrumental in completion of this thesis, completion of my course work, and successful navigation of the University and School's policies and processes. I would also like to thank the other members of my advisory committee, Dr. Mary Kasarda and Dr. Alan Kornhauser, for their time and detailed feedback on the work included in this thesis.

Second, I would like to thank the U.S. Coast Guard for providing me the opportunity to pursue a graduate degree. I look forward to employing what I have learned as a student at Virginia Tech to provide a positive return on the investment made by the Coast Guard and the taxpayers of the United States.

Finally, and most importantly, I would like to thank my wife and two boys for their unwavering support throughout my studies and career in general. I could not have accomplished what I have without their love and support.

Table of Contents

List of Figures

List of Tables

List of Abbreviations

B_2	Impeller Width (in)
C_b	Bearing Clearance, $C_b = R_b - R_j$ (in)
c_1	Lubricant Specific Heat Capacity (BTU/lb_m/ºF)
D_2	Impeller Diameter (in)
e	Eccentricity (in)
F_a	Aerodynamic Force (lb_f)
H	Heat Transfer Coefficient (BTU/in^2 ºF)
h	Lubricant Film Thickness (in)
K	Compressor Airflow Correction Factor (non-dimensional)
L	Bearing Length (in)
L_d	Distance from Center of Bearing to Center of Overhung Mass (in)
m_d	Overhung mass (lb_m)
N	Rotational Speed (revolutions per minute)
ΔP	Change in pressure between the centrifugal compressor inlet and discharge (psi)
Q	Compressor Capacity, Actual (ft^3/min)
Q_n	Compressor Capacity, Design (ft^3/min)
R_b	Bearing Radius (in)
R_j	Journal Radius (in)
T	Temperature of Journal (ºF)
U_m	Mechanical unbalance (oz-in)
U_t	Thermal unbalance (oz-in)

U_{thr}	Unbalance Threshold (oz-in)
W	Rotor weight (lb_f)
MCOS	Maximum continuous operating speed
α	Coefficient of Thermal Expansion (/ ºF)
ε	Eccentricity Ratio, $\varepsilon = e/C_b$ (non-dimensional)
ξ	Angle measured against rotation between hot spot on journal and line of centers (degrees)
θ	Angular distance between line of centers and the point of maximum film thickness (degrees)
μ	Lubricant Viscosity (Reyns)
ρ_l	Lubricant Density (lb_m/in^3)
ω	Rotational speed of rotor (radians per second)

1. Introduction

Supercharging is widely used in engine design to improve a given engine's power output. This performance enhancement is achieved by providing compressed air to the engine's cylinders to support combustion; the increased mass flow rate of air into each cylinder allows for the injection of larger quantities of fuel resulting in increased power production. A compressor driven by the engine's crankshaft via gears or a belt provides the increased airflow. Alternatively, engine exhaust is collected to drive a turbine that is mechanically connected to the compressor. This later arrangement is known as turbosupercharging, or more commonly turbocharging, while the term supercharging is typically reserved for the former mechanical drive arrangement.

Turbocharging is employed in spark-ignition engines in certain performance-oriented sports cars and many small compression ignition (diesel) engines used in light duty trucks. It is also widely used in large compression ignition engines in industrial applications where engine size is limited or where a turbocharger would improve engine performance such that fuel consumption may be decreased without reducing power output.

In each of these applications, a rotor consisting of a turbine and compressor rotates inside the turbocharger's housing. As it spins, the rotor vibrates as a result of its weight and weight distribution, material stiffness, aerodynamics of the turbine and compressor and their respective housings, and interaction with the rotor's support bearings. The study of these vibrations in rotating machinery is known as rotordynamics.

Many turbochargers are supported by fluid-film journal bearings with designs ranging from plain journal bearings to tilting-pad journal bearings. In automotive turbochargers, where production cost is a critical factor, inexpensive floating ring bearings are very common. In larger

engines, reliability and maintainability become more important than initial acquisition cost while the larger bearing loads caused by the heavier rotors drive a need for more advanced bearing designs.

The following analysis will analytically consider the use of floating ring bearings and tilting-pad journal bearings in a medium speed turbocharger that is representative of turbochargers used in marine propulsion applications aboard tug boats, buoy tenders, larger commercial fishing vessels, and similar working ships. As the rotor spins inside such turbochargers, heat is generated either through friction between rotating and stationary components or due to viscous shear in the fluid film supporting the rotor in the bearing. Under certain conditions, the rotor may be heated unevenly resulting in uneven bending of the rotor. This phenomenon is known as the Newkirk Effect in the case of frictional heat generation or the Morton Effect in the case of viscous shear heat generation. Particular attention will be given to the effect that changes in bearing geometry have on these thermal instabilities.

Finally, the interaction between the compressed air exiting a centrifugal compressor wheel and the compressor's volute will be considered. Such interaction, herein referred to as aerodynamic loading, may result in the development of forces several times higher than the static gravitational load of a rotor on its bearings. These loads will be analytically applied to the rotor-bearing system to consider the effect that the loads have on thermal instabilities.

1.1. Motivation

The focus of this analysis is the rotordynamics of turbochargers used in medium speed compression ignition engines for shipboard propulsion. These engines, and their turbochargers, are sufficiently large to produce significant bearing loads, yet cost is still a critical concern.

Engine loading is also highly variable much like an automotive engine versus the nearly constant engine load in many industrial applications such as power generation.

Reliability of marine turbochargers has also proven to be a concern for both the U.S. Navy and U.S. Coast Guard. While the total number of turbochargers in use in such environments is small compared to automotive or even typical industrial applications, and therefore frequently gains only marginal interest from manufacturers, the marine application introduces specific challenges. The study of these challenges will likely benefit turbocharger design as a whole and automotive applications in particular.

1.2. Thesis Outline

This thesis begins with a review of the basic theory necessary to consider the rotordynamics and thermal instabilities of marine turbochargers. Section 2 will also include a brief history of rotor dynamics and tribology. An analytical model of the Morton Effect specific to overhung bearings commonly found in small and medium sized turbochargers will then be presented in Section 3. This model will then be applied through use of computer software to analytically examine the presence of the Morton Effect in a typical marine turbocharger with various bearing geometries and varying aerodynamic loads.

2. Theory

Rotordynamics is the study of the motion of rotating mechanical devices. It is most commonly applied to analyze the vibrations of a spinning or rotating component of a machine such as an engine's crankshaft, a gas turbine, compressor, or turbocharger.

The rotating component of a machine is known as a rotor and may be a shaft, impellor, disk or similar device, or most commonly, a combination thereof. As the rotor spins it vibrates in lateral, axial, and torsional directions. Axial vibrations are those occurring parallel to the axis of rotation while lateral vibrations occur perpendicular to the axis of rotation and torsional vibrations occur in an angular direction about the axis of rotation.

2.1. Rotordynamics

The history of rotordynamics can be traced back to the work of W. J. M. Rankine, who is credited with documenting the first analysis of a spinning shaft in 1869 [1]. Unfortunately Rankine's model suggests that the radial deflection of a shaft increases without limit above a certain speed leading to the widely held belief at the time that operation above what is now known as the first critical speed would be unstable.

In 1895 Stanley Dunkerly published an analysis of shafts loaded by pulleys beginning his paper by stating "It is well known that every shaft, however nearly balanced, when driven at a particular speed, bends, and unless the amount of deflection be limited, might even break, although at higher speeds the shaft again runs true" [2]. Within these speed ranges, which he named critical speeds, large deflections of the rotor occur resulting in larger forces being transmitted to the support bearings. Dunkerley, however, did not hold the same stature as Rankine within science and engineering circles, and it was not until the practical work of W.

Kerr and Carl G. P. De Laval demonstrated that operation above the first critical was in fact feasible that the Royal Society of London hired Henry H. Jeffcott to resolve the conflict between Dunkerly's analysis and Rankine's analysis [3].

Jeffcott published his findings in 1919, and in doing so, promulgated what has come to be known as the "Jeffcott" or "Laval" Model of a rotor system. This model, shown in Figure 1, consists of a single disk, mounted equidistant between two identical, infinitely stiff bearings, on a uniform, flexible, massless shaft.

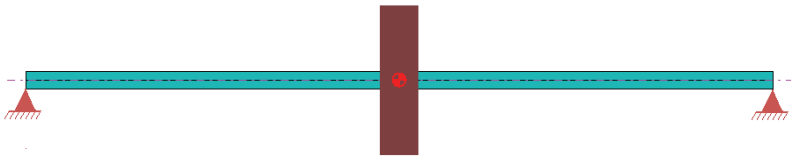

Figure 1: Jeffcott Rotor

This analysis provided an analytical explanation for De Laval's observations confirming that operation above the first critical was feasible and opened the possibility of designing rotors to operate at higher speeds. This model also provides an excellent model for examining basic rotordynamic theory that is still commonly used in both classrooms and technical papers.

2.2. Bearings

While the Jeffcott Rotor is useful for explaining basic rotordynamic theories, it is not a realistic model of any actual rotor systems due to the assumption of infinitely stiff supports (bearings) and a flexible shaft.

Bearings support and constrain the motion of moving components within a machine. In the case of rotating components, journal bearings support the rotor perpendicular to the axis of

rotation while thrust bearings constrain a rotor parallel to the axis of rotation. Bearings may be further divided into those where the journal and the bearing surface slide in relation to each other or those where the fixed (bearing side) surface and rotating (journal side) are separated by a rolling elements such as balls or cylinders. Fluid-film bearings, a subset of sliding surface bearings and the most common type of bearing in turbocharger applications, are designed to operate with a film of lubricant separating the journal from the bearing surface.

2.2.1. Bearing Geometries

The physical shape or geometry of the bearing is used to categorize sliding surface bearings. The most basic form is a 360-degree journal bearing which consists of a cylindrical sleeve fit about the journal surface. Modifications to this basic design, including addition of grooves, lobes, pockets and pivoting bearing surfaces are used meet specific application requirements.

The basic 360-degree journal bearing, or more commonly a plain journal bearing, is a fixed-geometry bearing as it does not have any mechanism to adjust for misalignment between the journal and bearing surfaces. Supply holes or grooves for lubrication are often added to the basic plain bearing geometry. For small bearings and bushings, a single supply hole may be used to inject lubricant near the center of the bearing and is most commonly situated 180 degrees from the load line or on the load line. Oil is then drawn and forced between the journal and bearing surface via hydrodynamic pumping or a hydrostatic external pressure source. A slight modification from the supply hole geometry is the use of grooves to improve transport of lubricants across the bearing surface. These grooves may be oriented parallel to the axis of rotation (axial grooves), perpendicular to the axis rotation (circumferential grooves), or in a spiral or helical pattern. Axial grooves are often placed opposite the load line or in pairs 90

degrees off the load line, with a length most commonly near 80% of the bearing length. Such an arrangement is particularly effective for ensuring adequate lubricant distribution across the length of the bearing when the load line is relatively constant. For cases where the load line changes in dynamically loaded bearings, a circumferential groove may be used to improve lubricant distribution. Finally, spiral and helical grooves are efficient ways of capitalizing on hydrodynamic pumping to lubricate a bearing in the absence of an external pressurized lubricant source. The fluid mechanics of lubricants in bearings are addressed in more detail in section 2.2.2.

The bearing may also be split such that is may be separated into two pieces allowing removal and replacement of the bearing without fully removing the rotor from the machine. Bearings may also be machined with a semi-elliptical geometry rather than a spherical geometry to produce an elliptical bearing or the bearing may be machined with three curved surfaces known as lobes or pads that are separated by grooves, both ways of reducing the circumferential whirl of oil which can cause dynamic instability in the bearing. Pressure dams or step journal bearings, which employ pockets cut into the bearing surface beginning at a groove or tapered from the bearing surface and with an abrupt edge on the trailing side of the pocket [4], may also be used to prevent the journal from developing an elliptical orbit within the bearing housing.

For cases requiring maximum reliability or where variable misalignment between the journal and bearing surface is expected, pivoted-pad or tilting pad bearings may be used. In theses bearings, a number of pads are supported within the bearing housing by a ball, cylinder, or similar lobe which allows each pad to pivot with one or more degrees of freedom in order to align itself with the journal.

2.2.2. Fluid Film Dynamics

The purpose of a lubricant is to control friction and wear between surfaces while removing heat and wear particles. In the case of fluid-film bearings, the lubricant is typically oil or water. Most oils used in lubrication of bearings are derived from refined petroleum but synthetic oils are also used in particularly demanding applications.

The study of journal bearings designed to operate with a film of lubricant separating the journal from the bearing surface began during the mid-1800's with the work of F. A. von Pauli and G. A. Hirn. N. P. Petrof followed in 1883 with examinations of the work of Hirn as well as that of H. Kirchwerger who focused on bearing materials in railway axle bearings, R. H. Thurston who experimentally considered friction in bearings, and M. Margules's hydrodynamic theory, to conclude that bearing friction was a hydrodynamic phenomenon [5].

In 1885, Beauchamp Tower published his experimental results examining oil lubricated journal bearings, which demonstrated the existence of hydrodynamic pressure in a bearing's lubricant film. The following year, Osbourne Reynolds published his celebrated analytical paper [6] reviewing and analyzing the results of Tower's experimentation. In this analysis, Reynolds derived a simplified version of the Navier-Stokes Equations, the elegant yet virtually unsolvable set of three, second-order, non-linear, partial differential equations used to mathematically describe fluid flow. This provided an analytical explanation for hydrodynamic lubrication that continues to serve as the foundation for lubrication theory.

Solving Reynolds Equation results in the hydrodynamic pressure distribution resulting from the convergence and normal forces between the bearing and journal surfaces. Figure 2 depicts the pressure distribution in a plain journal bearing.

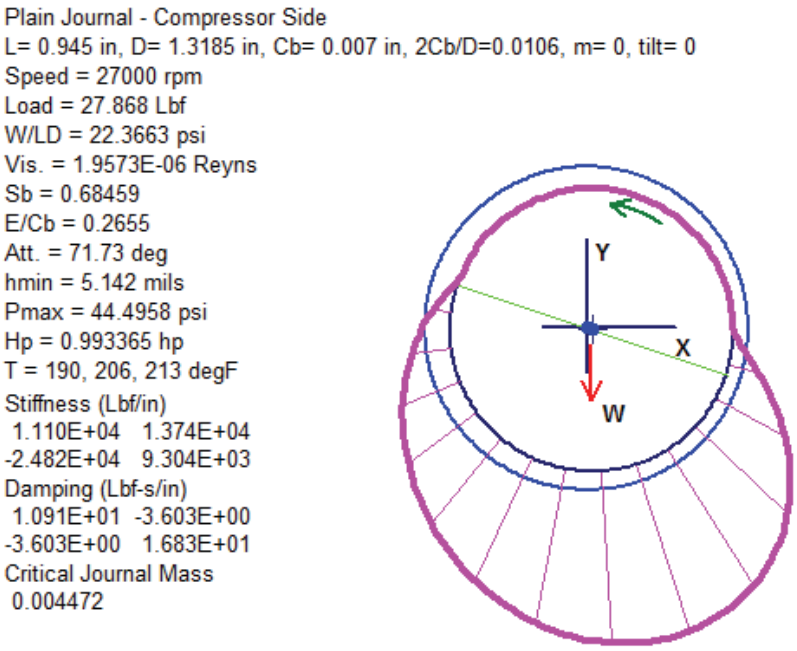

Figure 2: Hydrodynamic Pressure Profile in a Plain Journal Bearing

Note that the axis of rotation of the rotor (the blue dot in Figure 2) is slightly below and to the right of the center of the bearing shown as a cross. Assuming a stationary shaft and 0 psi at the lube oil inlet, the shaft would rest at the bottom of the bearing. As the shaft begins to rotate, lube oil contacting the journal surface rotates with the surface with no slip. Within this area, the converging surfaces of the bearing surface and journal surface, coupled with the lube oil flowing into the convergence, results in the development of a positive pressure gradient that separates the two surfaces. A negative pressure gradient follows in the lower right quadrant as the diverging surfaces have an opposite effect.

This pressure field provides the forces that support the rotor's journal within the bearing. If an external force displaces the journal, the pressure field will exert a restoring force in the opposite direction. This restoring force divided by the displacement is known as the bearing stiffness. The fluid film will also resist changes in the journal's position. This resistance, which

is proportional to the velocity, is known as damping. As discussed above, the center of the journal usually shifts from the bearing center. If the journal is then displaced in the vertical direction the fluid film will resist the displacement with vertical and horizontal components. The restoring force acting perpendicular to the displacement divided by the displacement is the cross coupled stiffness.

2.3. Thermal Instabilities

At the same time Jeffcott provided an analytical explanation for De Laval and Kerr's practical demonstrations, the quest for improved efficiency encouraged reductions in weight. This resulted in more flexible rotors and support structures while operating speeds increased opening the divide between Jeffcott's model and modern rotor-bearing systems. Numerous failures followed that contemporary engineers could not explain using existing theory.

In response to these failures, B. L. Newkirk, in his work for General Electric [7], conducted a series of experiments during the early 1920's finding that the axis of rotation of the rotor would begin to orbit within the bearings when the rotor was operated above the first critical. He noted that if the shaft orbited synchronously, or in other words that the speed at which the shaft progressed about the orbit was the same as the speed of rotation of the shaft, that the same point of the shaft would always present itself at any given point about the bearing. Figure 3 provides an example of a synchronously whirling shaft. The ellipse shown in both plots represents the path of the center of the journal as it orbits within the bearing housing while the journal is represented by the small circle shown at the upper and lower extents of the ellipse in the left and right plots, respectively. Each small circle includes a line from the center to the same point on the circumference to show orientation of the journal. Two speeds are important here; the speed at which the journal orbits about the bearing in its elliptical path and the speed at which

the journal itself spins. In synchronous whirl, these two speeds are the same resulting in the same point of the journal always presenting itself to the inside of the orbit and the opposite point on the journal always pointing outwards towards the bearing housing. This is shown in Figure 3 where the point 45 degrees before, as measured counter-clockwise from the line connecting the center of the journal and the circumference, always points away from the center of the plot.

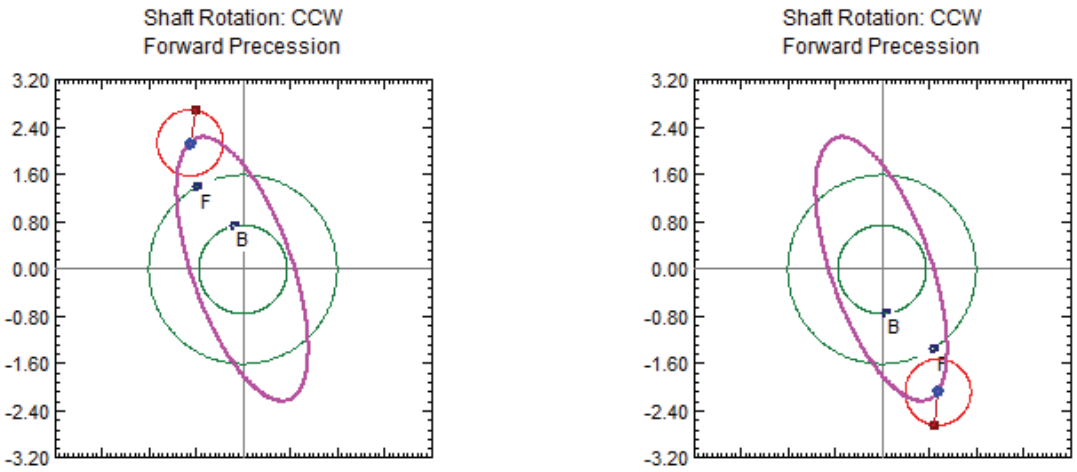

Figure 3: Synchronous Whirl

If the size of the orbit was sufficiently large such that components of the rotor contact fixed components under these conditions, frictionally induced localized heating of the shaft would occur. The localized heating would then result in thermal bending of the shaft leading to growth in the size of the orbit. This growth would exacerbate the frictionally-induced heating in a self-perpetuating cycle until rotor or bearing failure occurred through the process now known as the Newkirk Effect. A. J. Kimball, also of the General Electric Company's Research Laboratory, advanced a separate theory that the whirling motion of the shaft could also be the result of internal friction originating from relative movement between the shaft of a rotor and components that are shrink fit about the shaft and flexural stresses within the material of the rotor.

Kroon and Williams attempted to develop an analytical model of the Newkirk Effect in 1939 and what they called "spiral vibrations" in reference to the circular loops of the unbalance response of the rotor as shown on a polar plot. However, it wasn't until 1973 that A. D. Dimaroganonas developed and experimentally tested analytical models of the Newkirk Effect [8] utilizing recent advances in vibration sensors to accurately capture the behavior of the rotor. W. Kellenberger continued efforts to quantitatively describe the phenomenon while focusing specifically on ring seals as the cause of frictionally-induced heating [9]. J. Schmied introduced finite element methods in 1987 [10] to examine spiral vibrations in both a simple flexible rotor model and a practical turbine generator model.

At the same time Dimarogonas was working with the Newkirk Effect, P. G. Morton and B. Hesseborn were separately examining localized rotor heating resulting from temperature gradients in the lubricant film [11] rather than physical contact between the rotor and support structures. Although Schmied considered this thermal-hydrodynamic effect with approximations in his model of the Newkirk Effect, it wasn't until P. S. Keogh and Morton published their findings in 1993 [12] and 1994 [13] that a full examination of the Morton Effect, as it has come to be known, was made public.

A. C. Balbahadur [14] modified Keogh and Morton's analytical model and converted it from one that is frequency based to one that is time based in an effort to make the model more user friendly for design purposes. Z. Guo [15-17] further improved upon Balbahadur's work by examining instances of the Morton Effect in mid-span rotors, a departure from previous experimentation and analyses that considered the presence of the Morton Effect in bearings supporting overhung masses. Based on the results of the two previous efforts, Kirk, Guo, and

Balbahadur automated application of the models with the computer code and supporting graphical-user interface, known as VT-MAP [18], utilized in this analysis.

The principle difference between the Newkirk Effect and the Morton Effect is that the rotor does not make physical contact with the fixed support structure such as a bearing or ring seal in the Morton Effect. Instead of physical contact, variations in the amount of viscous shear of the lubricant film caused by the journal's orbit, results in uneven heating of the journal. This localized heating, whether through physical contact or viscous shear, causes the rotor shaft to bend through localized thermal expansion. This bending leads to growth of the orbit resulting in increased friction or viscous shear leading to further bending. This cycle continues until the bearing or rotor fails or the machine is shut down due to excessive vibration.

3. Analytical Model

Modeling of thermal instabilities begins with modeling the steady-state response of the rotor-bearing system. This steady-state response is a function of external excitation and self-excitation. External excitations are the source of vibrations where the source exists in the static rotor such as mass unbalance and gravitational forces or may be a forced response to vibration of a nearby machine or the motion of the vessel through the rotor's foundation in marine applications. In contrast, self-excitation sources are a result of the movement of the rotor such as hydrodynamic cross-coupling in bearings and aerodynamic cross coupling. Essentially, sources of external excitation are measurable in a rotor at rest while self-excitation sources do not manifest themselves until the rotor is spinning.

3.1. External Excitation:

The principal source of external excitation to be considered in this analysis is mass unbalance. Every rotor will invariably have some mass unbalance either as the result of design characteristics such as keyways, as a result of material inconsistencies, or as the result of machining. As would be expected, mass unbalance resulting from other than design characteristics varies between otherwise identical rotors. Therefore, the generic mass unbalance presented by Balbahadur and Kirk [19] that is based on the assumed mass unbalance used in early versions of the American Petroleum Institute's Standard 617 for centrifugal compressors [20], is assumed for modeling purposes

$$U_m = \frac{56{,}347W}{N_{MCOS}^2} = \frac{617.9W}{\omega_{MCOS}^2} \qquad (1)$$

where W is the weight of the rotor (lb_f), N_{MCOS}^2 is the squared rotational speed of the rotor in revolutions per minute at the rotor's design maximum continuous operating speed, ω_{MCOS}^2 is the

squared rotational speed of the rotor in rad/s^2 at the rotor's design maximum continuous operating speed, and U_m is the mass unbalance in oz-in. This unbalance, which is based on the unbalance required to produce a force equal to 10% of the rotor weight, is assumed to act at the center of mass in the overhung portions of the rotor.

3.2. Self Excitation:

Typical sources of self-excitation include rotor damping, magnetic fields, aerodynamics, and most commonly, fluid film bearings.

Rotor damping is the combined effect of friction between the shaft of a rotor and components that are shrink fit about the shaft and flexural stresses within the material or the rotor itself. This form of self-excitation, as well excitations caused by magnetic fields, are ignored in this analysis.

Aerodynamic excitation is the result of interaction between the rotor and its gaseous environment. While air will interact with a rotating cylindrical shaft or plain disk, the numerically significant interaction in a turbocharger's rotor occurs in the turbine and compressor wheels. The magnitude and direction of the forces generated in a compressor wheel is a function of the design of both the impeller and housing. In this analysis, a centrifugal impeller is assumed to operate inside a single-volute casing. The magnitude of the force may then be estimated using a variation of the equation for radial thrust in a volute casing presented by Stepanoff [21]:

$$F_a = \frac{KHD_2B_2}{2.31} \approx KD_2B_2\Delta P \qquad (2)$$

where F_a is the radial force, in pounds, ΔP is the change in pressure between the compressor inlet and discharge in psi, D_2 is the impeller diameter, in inches, B_2 is the impeller width, in

inches, and K is a constant accounting for the airflow through the compressor versus the design capacity. K may be roughly approximated by the following:

$$K = 0.36\left[1 - \left(\frac{Q}{Q_n}\right)^2\right] \quad (3)$$

Stepanoff [21] found that the direction of this force typically begins 10 to 20 degrees past the volute discharge in the direction of compressor rotation and shifts 100 to 180 degrees as rotation speed and therefore airflow increases.

Finally, fluid film bearings introduce what is typically the greatest source of self-excitation. When the center of the journal shifts away from the center of the bearing, due to viscous forces in the oil, mass unbalance of the shaft, or an external excitation, the pressure field developed in the lubricating oil provides a restoring force. However, this restoring force is not aligned with the line of displacement between the journal and bearing center. Instead, the cross-coupled stiffness, as discussed in section 2.2.2, results in a shift in the direction of the restoring force leading to the development of an elliptical orbit of the journal within the bearing.

The mass unbalance, as well we the sources of self-excitation discussed above, will result in a spiral vibration where the axis of rotation of the shaft elliptically orbits about the center of the bearing. The center of the orbit may be found using Cameron's [5] approximation for film thickness:

$$h = C_b(1 + \varepsilon\cos\theta) \quad (4)$$

where C_b is the radial clearance, ε is the eccentricity ratio, e/c_b, where e is the distance between the center of the shaft and the center of the bearing, and θ is the angle between the line of centers and the point of maximum film thickness. The static equilibrium position of the shaft may then be determined based on the film thickness, journal geometry, and bearing geometry

through trigonometry. This static equilibrium point is the axis about which a theoretical shaft with no internal or external excitation would rotate. In an actual shaft, which invariably has a finite mass unbalance, this equilibrium position is the point about which a shaft vibrates.

3.3. Thermal Effects

As the rotor journal travels synchronously about this orbit, the journal is heated unevenly. To model this uneven heating, the overhung mass supported by the bearing is treated as a cantilever beam and the thermal bending moment is depicted similar to the bending moment. Balbahadur and Kirk [19] derived this thermal bending moment, U_t, resulting in the approximation:

$$U_t = m_d \frac{\alpha \Delta T}{R_j} L L_d \qquad (5)$$

where m_d is the overhung mass, α is the coefficient of thermal expansion of the journal, ΔT is the average temperature difference between the hot spot and cold spot, R_j is the journal radius, L is bearing length and L_d is the distance from the center of the bearing to the center of the overhung mass.

The average temperature difference between the hot and cold spot in eq (5), ΔT, is found by solving for the temperature distribution in the lubricant film:

$$\frac{dT}{d\xi} + \frac{2HT}{\rho_l c_l \omega h} - \left(\frac{2HT_{amb}}{\rho_l c_l \omega h} + \frac{2\mu\omega R_j^2}{\rho_l c_l h^2} \right) = 0 \qquad (6)$$

where T is the temperature of the journal, ξ is the angle between the hot spot and the line of centers connecting the journal center and bearing center, as measured against rotation, H is the heat transfer coefficient, ρ_l is the lubricant density, c_l is the lubricant specific heat capacity, μ is the lubricant viscosity, and R_j is the journal radius. Balbahadur and Kirk [19] derived this

equation by assuming a steady-state energy balance which neglects axial heat flow, assumes that the viscous energy heats the lubricant or is transferred to the journal or bearing housing, and assumes a Newtonian fluid with a linear velocity profile.

The total unbalance may then be determined by considering the thermal and mechanical unbalances and accounting for the difference in their respective phase angles:

$$U = \sqrt{U_t^2 + U_m^2 - 2U_t U_m \cos\left(\omega t - \theta_{CH}\right)} \qquad (7)$$

Finally, the Morton Effect is assumed to result in unstable operation when this total unbalance exceeds a threshold value. Experimental results analyzed by Balbahadur [14] demonstrated that this threshold value is approximately equal 15% of the rotor weight:

$$U_{thr} = \frac{84520W}{N^2} = \frac{926.85W}{\omega^2} \qquad (8)$$

Where N^2 is the variable rotor speed in revolutions per minute and ω^2 is the variable rotor speed in radians per second.

Guo later revised the threshold to better predict onset of the Morton Effect independent of the specific rotor-bearing configuration over a wider speed range:

$$U_{thr} = 1.5U_m \qquad (9)$$

Both models assume that when the total unbalance exceeds the initial mechanical unbalance by 50%, the system will be unstable, but differ in the dependence on rotor speed. The effect of this difference is depicted in Figure 4. The plot assumes a 10 lb_f rotor that operates at a maximum continuous speed of 50,000 rpm. The horizontal dashed line at $2.25*10^{-4}$ oz-in is the assumed mass unbalance given by eq (1), the solid horizontal line at $3.38*10^{-4}$ oz-in is the threshold predicted using Guo's model (eq (9)), and the dashed line falling to the right is the threshold predicted by Balbahadur's model (eq (8)).

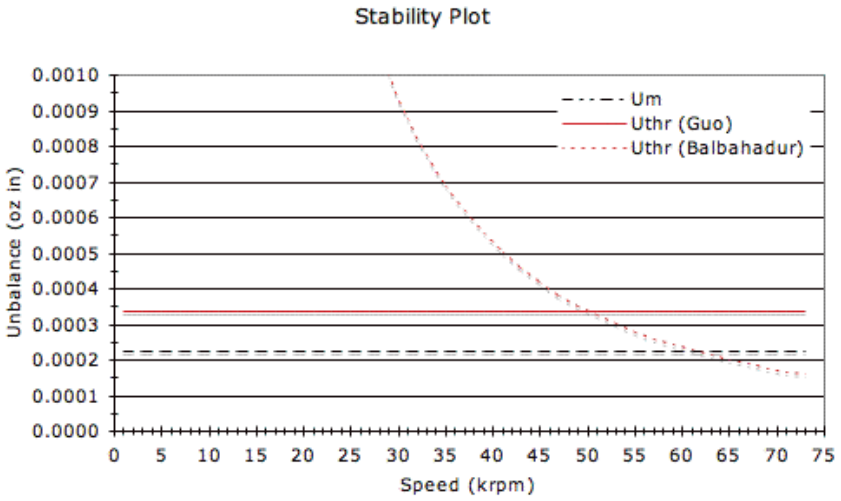

Figure 4: Comparison of Stability Threshold Formulas

Balbahadur's model was developed with an emphasis on slow speed rotors and is based on the formula for assumed mass unbalance used in damped unbalance response analyses presented in early versions of API Specification 617 [20]. As speeds increased beyond 12,000 rpm with efforts to improve machine efficiency in centrifugal compressors, however, the American Petroleum Institute acknowledged that the model was unsatisfactory. Guo's model provides a suitable alternative, particularly for machines operating above 12,000 rpm, to address this issue in the underlying formula used by Balbahadur.

The mass unbalance, total unbalance, and threshold are then plotted against rotational speed in a manner similar to Figure 4. Deviations in the total unbalance from the mechanical unbalance indicate thermal bending is occurring as a result of the Morton Effect. Areas where the total unbalance exceeds the threshold indicate an unstable system where the total unbalance is sufficiently large to produce damaging vibrations.

4. Turbocharger Model

4.1. Turbocharger Rotor

For the purpose of this analysis, a double-overhung turbocharger with a centrifugal compressor and axial turbine supported by oil lubricated journal bearings is assumed. The turbocharger's rotor, depicted in Figure 5 below, consists of a compressor shaft and a turbine shaft joined via a threaded and tapered connection that is locked in place via a tie bolt. An inducer and centrifugal compressor are fit on the compressor shaft and held in place by the nose cone that is threaded into the inside of the compressor shaft. The axial turbine, which is cast and then friction welded to the turbine shaft, is considered an integral part of the turbine shaft. Finally, a thrust collar is fit about the shaft near the overall rotor's center of gravity.

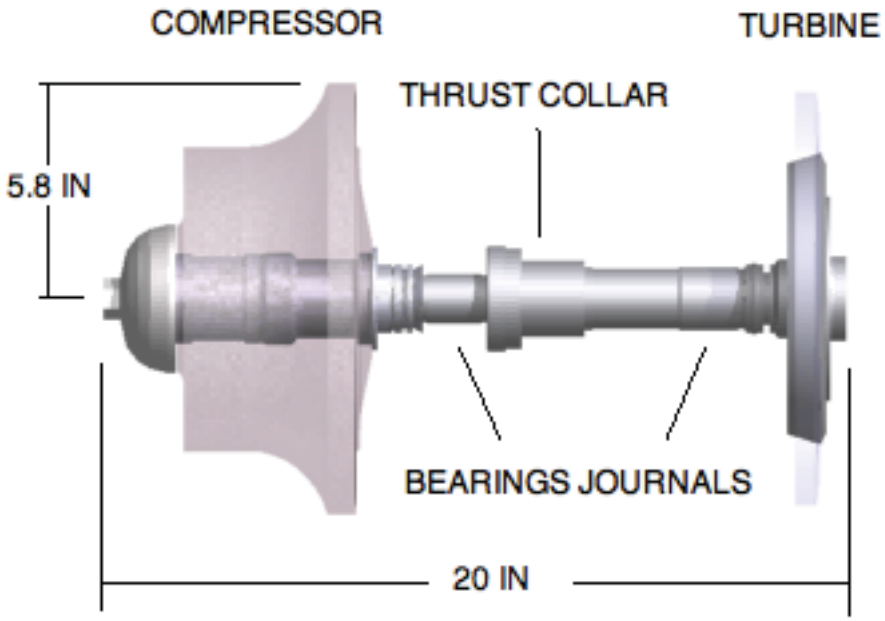

Figure 5: Turbocharger Rotor

The turbocharger was modeled using version 13.01 of the commercially available software tool DyRoBeS [22]. DyRoBeS utilizes finite element methods to complete rotordynamic analyses and bearing performance calculations using the ROTOR and BePerf portions of the software suite, respectively. Figure 6 below, shows the DyRoBeS ROTOR model:

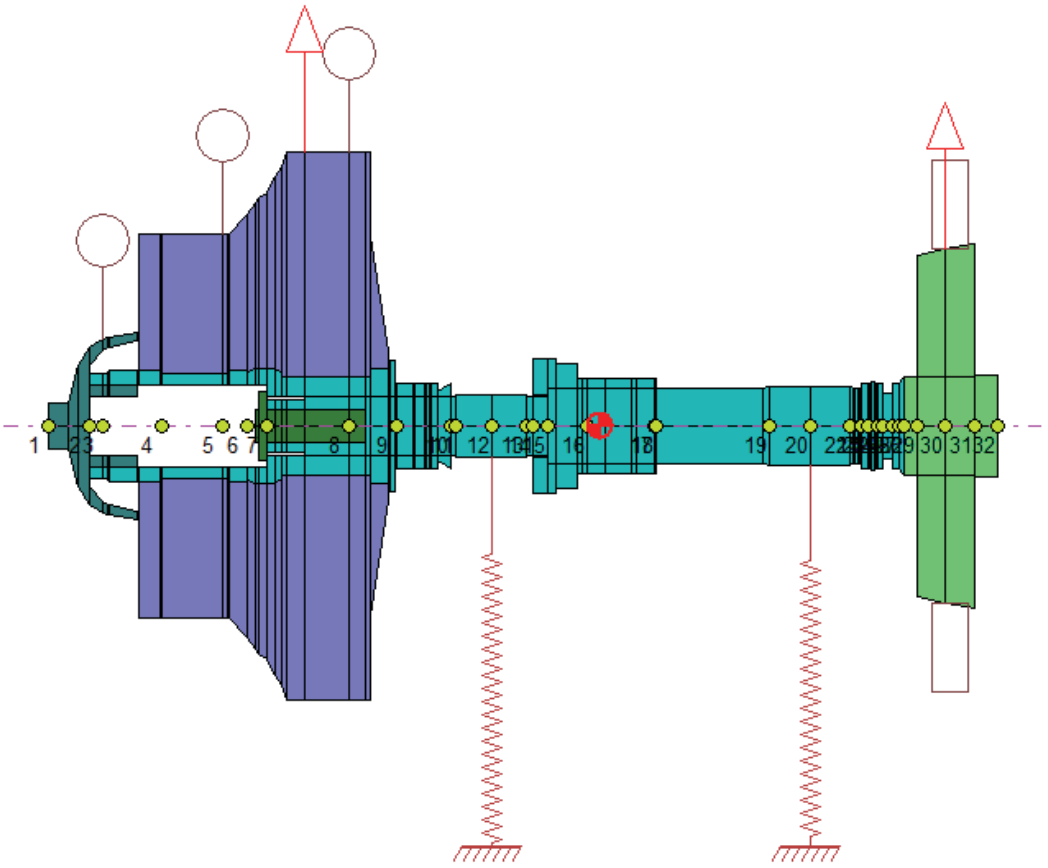

Figure 6: Turbocharger Rotor Model

This model is composed of a steel turbine shaft and steel compressor shaft matching the rotor in Figure 5. The compressor and turbine were then included in this computer model using materials reflecting the stiffness of aluminum and steel respectively, but with zero mass allowing addition of inertial and mass properties separately. The circular markers above the rotor and the

rectangular markers above and below the turbine disk indicate the location of disks added to account for the inertial and mass properties while the triangular markers indicate the location of mechanical unbalance forces.

This turbocharger rotor weighs 42.5 lb_f resulting in static loads of 27.9 lb_f and 14.6 lb_s at the compressor and turbine bearings, respectively, and typically operates between 14,000 and 30,000 rpm. Analysis of the Morton Effect will concentrate on the compressor-end bearing where the compressor wheel and associated shafting constitute a 20.1 lb_m overhung mass with a center of gravity 4 inches outboard of the center of the bearing. Complete model details are included in Appendix A.

4.2. Aerodynamic Loading

To consider the aerodynamic effects, a representative turbocharger characteristic map and a typical shipboard engine load line for a single-shaft, fixed-pitch propeller system were overlaid in a process similar to what would be completed in an engine and turbocharger matching process.

Compressor characteristic maps generally show the pressure ratio (discharge pressure divided by inlet pressure) of a compressor versus the mass or volumetric flow rate of gas through the compressor. Lines of constant rotor speeds are then plotted to show the pressure ratio as a function of the gas flow rate at each given speed. Finally, lines of constant isentropic efficiency, which assume the air is compressed in a reversible process without dissipation of energy and assume no loss of thermal energy (adiabatic process) are added to the plot. Generally, a designer attempts to operate the compressor at the highest efficiency possible without driving the compressor into the surge region where local flow of the gas reverses in the compressor due to excessive pressure ratios and low flow rates.

Turbomachinery, such as compressors and turbines, are most efficient in a small range of speeds and gas flow rates where the angles at which the gas enter or exit a compressor or turbine most closely match the blades angles of the inducer, compressor, or turbine. In contrast, engines often operate over a large range of speeds producing varying flow rates of exhaust with angles of flow that depart the optimal conditions in the turbocharger depending on engine speed and load. To address this difference, turbochargers are matched to engines to maximize the range of engine speeds and loads where efficiency of the turbocharger is maximized and where normal operation is not expected to drive the compressor into surge.

To match the modeled turbocharger to a marine propulsion engine, a single-shaft, fixed-pitch propeller system was selected for simplicity. In a fixed pitch propeller system, the engine load is proportional to the cube of the ship's propeller speed producing a single operating line reflecting engine speed and load that may be plotted over the compressor characteristic map. The same engine to turbocharger matching process would apply for other shipboard configurations including use of controllable pitch propellers or multiple engines driving a single propeller shaft. These changes would simply result in altered engine load lines based on the specific arrangement. For additional information, Watson [23] provides an excellent discussion of this matching process and typical engine load lines for various shipboard configurations.

To model the aerodynamic effects on the modeled turbocharger, the assumed engine load line was overlaid on a compressor map for a turbocharger compressor with dimensions matching the modeled turbocharger rotor. The volumetric flow versus rotor speed where then read along the engine load line and the pressure ratio versus volumetric flow were determined to develop a plot of flow rate of air through the compressor versus turbocharger speed:

$$Q = 3.4398E-09 \cdot N^2 + 9.8699E-06 \cdot N \qquad (10)$$

where N is the rotor speed in revolutions per minute.

It was then assumed that the turbocharger was designed to operate at 30,000 rpm allowing calculation of values for the correction factor K (eq (3)) over the operating range of the compressor. Finally, these values for K and the pressure ratios at each speed point were entered into the equation for aerodynamic force (eq (2)) to develop a representative curve of aerodynamic force versus rotor speed:

$$F_a = -9.3572238E-07 \cdot N^2 + 3.8046682E-02 \cdot N - 2.7933533E+02 \qquad (11)$$

This aerodynamic force was then applied as a bearing load on the compressor end bearing for bearing stiffness and damping calculations and at the center of the shaft in line with the compressor wheel's discharge (station 8 in Figure 6). While this force would actually act on the rotor at the compressor discharge, the lever arm was ignored in bearing calculations due to the very rough approximation methods used to determine the force itself. Aerodynamic loading of the axial turbine bearing was ignored. DyRoBeS' BePerf Application and VT-MAP allow for the application of a speed dependent load in the form of equation (11) but DyRoBeS ROTOR does not. Instead, a constant force of 90 lb_f was applied at station 8 at 270 degrees.

4.3. Morton Effect

Thermal bending in the compressor bearing was analyzed using the Virginia Tech Morton Analysis Program (VT-MAP) [18]. This software predicts if a given fluid-film bearing system will exhibit the Morton Effect and is capable of analyzing fixed and variable geometry journal bearings in turbo machinery with overhung and center hung masses.

The VT-MAP thermal effects analysis is based on the following inputs:

Table 1: Data for Turbocharger Compressor Bearing

Lubricant Properties			
	Density	ρ_l	0.031 lb/in^3
	Specific Heat Capacity	c_l	0.499 BTU/lb$_m$/ºF
	Supply Viscosity	μ	2.56*10^{-6} Reyns
	Supply Temperature	T_0	190 ºF
	Ambient Temperature	T_{amb}	100 ºF
	Thermoviscosity Coefficient	β	0.016 / ºF

Rotor Properties			
	Rotor Weight	W	42.51 lb$_f$
	Overhung Mass	M_d	20.148 lb$_f$
	Overhung Distance	L_d	3.975 in
	Initial Mechanical Unbalance	U_M	0.00266 oz in
	Maximum Continuous Operating Speed	ω_{MCOS}	3141.593 rad/s

4.4. Analysis Methodology

To complete the analysis, bearings were modeled using the BePerf portion of DyRoBeS to model the resulting stiffness and damping characteristics of the given bearing configuration. Details of each bearing system, which were varied as part of this analysis, are included in section 5. The stiffness and damping characteristics were then applied to the rotor model in the ROTOR portion of DyRoBeS to consider the amplitude and phase of the resulting synchronous, steady-state,response of the rotor across the operating speed range. These amplitude and phase angles were then entered into VT-MAP for analysis to determine if the Morton Effect would drive the rotor-bearing system unstable.

Each model assumes the same static loading characteristics and the use of a typical SAE-40 lubricating oil with a supply temperature of 190 ºF and an ambient temperature of 100 ºF. While these conditions are not extreme for a shipboard engineering environment, they are on the upper end of what one would typically find. Bearing geometry and aerodynamic loading were then varied to consider the impact of geometry and bearing loads on thermal instability.

5. Results

To consider the impacts of bearing geometry and aerodynamic loading on the Morton Effect, the use of floating ring and tilting pad journal bearings are considered with the turbocharger rotor described in section 4.1. Floating Ring Bearings are common in high-speed automotive turbocharger applications while tilting-pad journal bearings become more common in larger turbochargers where reliability of the equipment becomes a greater concern than initial production cost. For each bearing configuration, an analysis of the lateral vibration and stability of the rotor-bearing system is presented followed by a thermal stability analysis. Aerodynamic loading is then applied to the rotor-bearing system to consider the impact on lateral and thermal stability.

5.1. Turbocharger with Floating Ring Journal Bearings

A floating ring bearing is a style of journal bearing that includes a free-floating ring, or bushing, suspended within a fluid film between the journal and bearing housing. The rotating shaft (journal) is supported within the floating ring by a fluid film while the ring is suspended within the bearing housing by a fluid film. This essentially creates a plain journal bearing within a plain journal bearing except that the ring is allowed to rotate about the shaft's axis of rotation.

Floating ring journal bearings are common in small, high-speed turbochargers. The bearings are relatively inexpensive to produce and require relatively small bearing housings allowing for construction of smaller machines. This compact size is important in mobile application such as automotive or truck engines where space is limited and where reduction of weight may allow for increased cargo capacity or reduced fuel consumption.

The floating ring bearing model used in this analysis, as shown in Figure 7, assumes the bearing characteristics in Table 2.

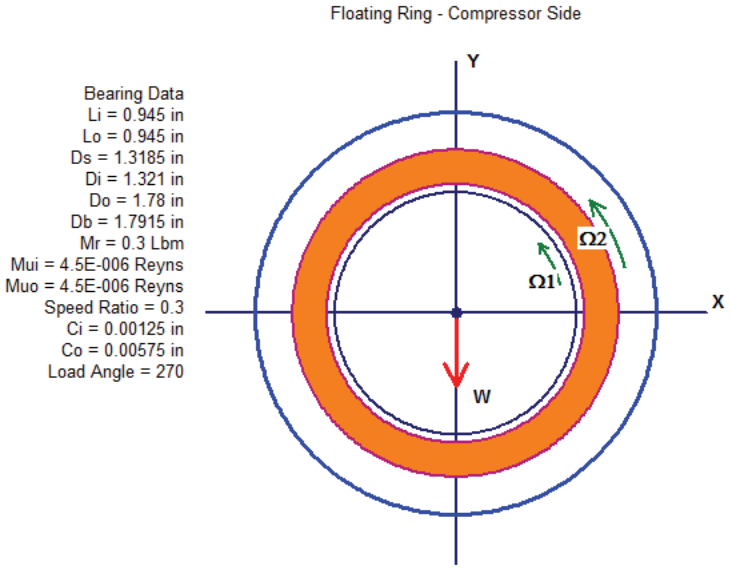

Figure 7: Floating Ring Journal Bearing Model

Table 2: Bearing Characteristics: Floating Ring Journal Bearing

Bearing Property		Compressor	Turbine
Journal Radius (in)	R_j	1.3815	1.6925
Bearing Length (in)	L	0.945	0.985
Radial Clearance – Inner (mil)	C_b	1.250	1.400
Radial Clearance - Outer (mil)	C_b	5.750	4.500
Heat Transfer Coefficient (HP/in^2/ºF)	H	$2.435*10^{-6}$	$2.435*10^{-6}$
Journal Coefficient of Thermal Expansion (/ ºF)	α	$6.11*10^{-6}$	$6.11*10^{-6}$
Gravity Load on Bearing (lb_f)	W_b	27.868	14. 640

To consider the suitability of this bearing configuration for the turbocharger rotor, a lateral stability analysis was completed while ignoring aerodynamic loading and the possibility of thermal bending. Figure 8 graphically presents the results of that analysis in the form of logarithmic (log) decrement versus rotor speed, indicating an unstable configuration.

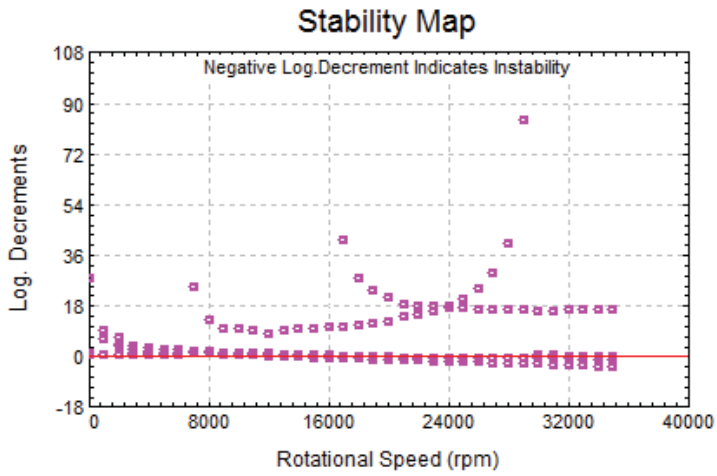

Figure 8: Lateral Stability Map for Floating Ring Bearing

Log decrement is a measure of the change in amplitude of successive oscillations of a vibration; positive values indicate a stable system while negative values indicate increasing amplitudes and therefore an unstable system. To create the plot shown in Figure 8, the log decrement was calculated for each of the first three real modes for rotor speeds between 0 and 35,000 rpm at 1000 rpm intervals. It should be noted, however, that the unloaded condition assumed when developing Figure 8 is a theoretical situation that would not be possible in a machine that is powered by exhaust gas an engine's cylinders.

A lateral critical speed analysis of the rotor-bearing system indicates that the turbocharger will operate between the second and third criticals. The three curves rising from the left side of the plot reflect the first three modes versus bearing stiffness while the line falling from the left reflects the average direct stiffness (Kxx+Kyy)/2 of the compressor end bearing. The horizontal dashed lines at 14,000 and 30,000 rpm reflect the anticipated upper and lower operating limits of the turbocharger.

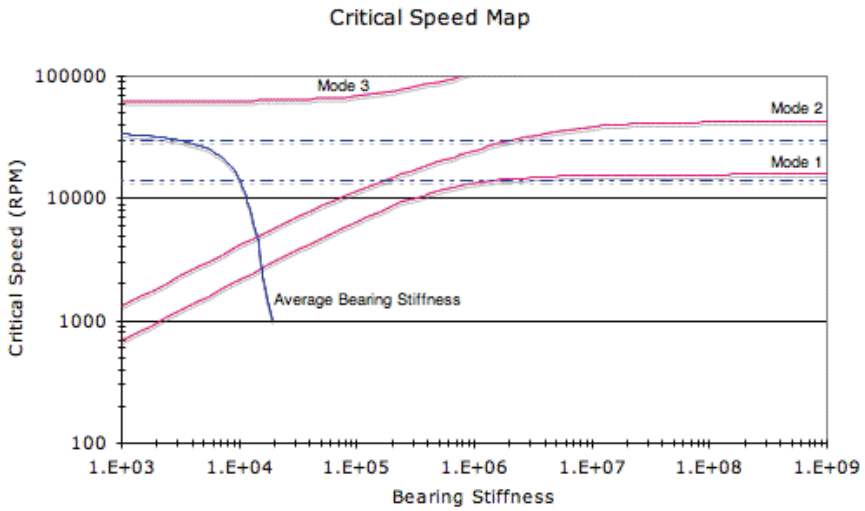

Figure 9: Critical Speed Map - Turbocharger with Floating Ring Bearings (1.5mil Clearance)

This plot indicates that this rotor-bearing system is expected to pass through the first two modes and operate below the third mode, with adequate margins between the expected operating range and the critical speeds.

A waterfall plot, Figure 10, was then developed from a time transient response analysis completed at constant speeds to consider the response of the rotor-bearing system at speeds of 2,000 rpm to 34,000 rpm in 2,000 rpm increments. The diagram is very helpful in identifying the presence of half-frequency excitations (0.5x) often caused by oil whirl and synchronous excitations (1.0x) caused by unbalances. The plot was generated in MATLAB [24] following a procedure developed by Alsaeed [25] to plot the Fast Fourier Transform (FFT) Spectrum output of DyRoBeS® ROTOR.

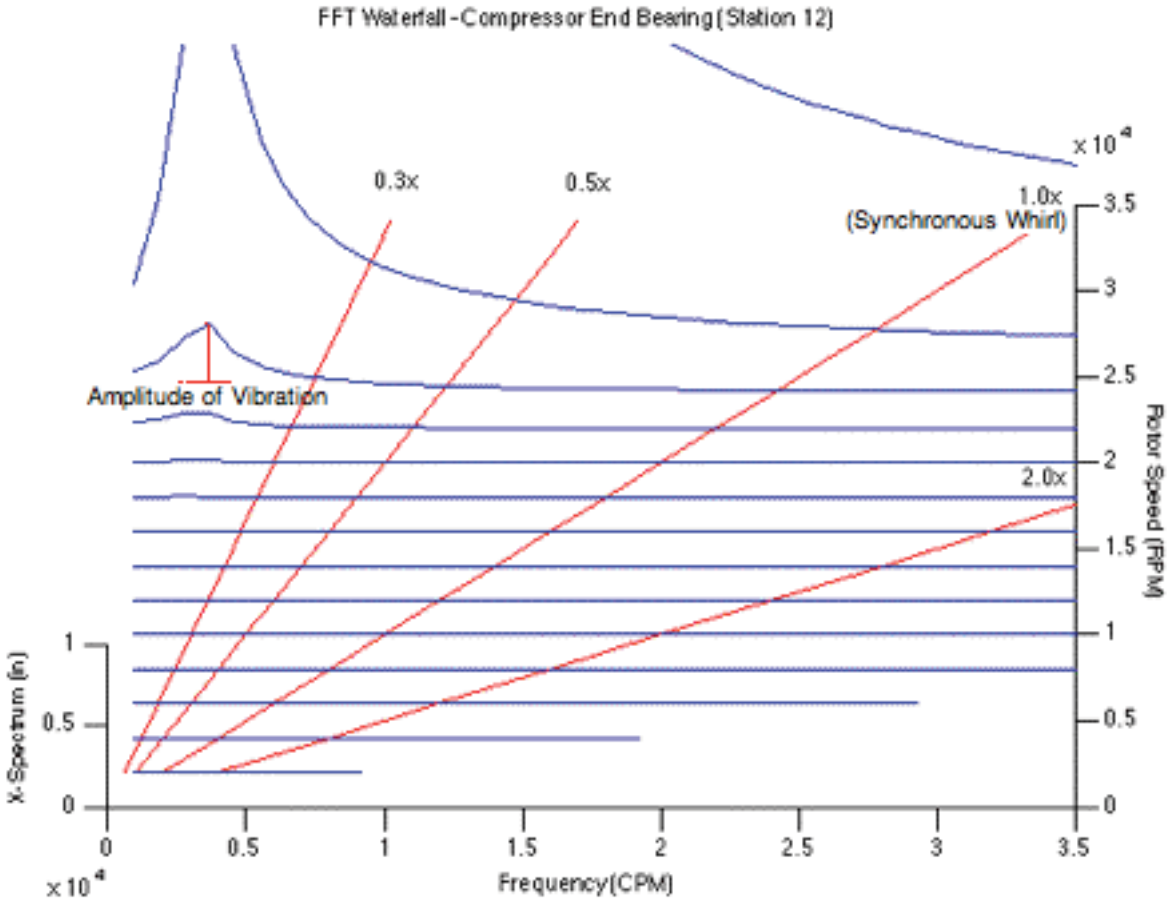

Figure 10: Waterfall Plot: Turbocharger with Unloaded Floating Ring Bearings (X-dimension at Compressor Bearing)

Each horizontal line in a waterfall plot reflects the response spectrum at a given rotor speed allowing the frequency components of vibration to be determined. Mountains in the horizontal lines indicate the frequency component; peaks slightly to the left of the 0.5x line would indicate that oil whirl in the fluid film bearings is exciting the rotor while peaks near the 1.0x synchronous line would indicate that unbalance is contributing to the vibration of the rotor.

The absence of synchronous response (1.0x) in Figure 10 indicates that thermal instabilities are unlikely. VT-MAP confirms these preliminary findings, as shown in Figure 11, indicating that this rotor-bearing system is not expected to exhibit the Morton Effect over the entire operating range of the turbocharger. The solid blue line represents the expected total

(mass plus thermal) unbalance, eq (7), expected in the rotor-bearing system. The upper horizontal dashed line at 0.004 oz-in in this plot represents the thermal instability threshold, eq (9), while the lower dashed line at 0.003 oz-in represents the initial mechanical unbalance, eq (1).

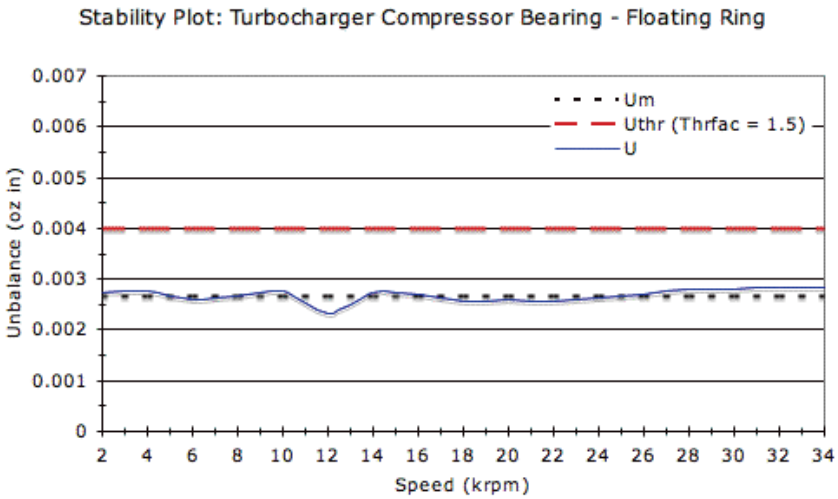

Figure 11: Thermal Stability Plot: Turbocharger with Unloaded Floating Ring Journal Bearings (1.25 mil Inner Clearance)

The assumed radial clearance between the journal and floating ring was then altered to consider the impact of changes in geometry of floating ring bearings on the thermal stability of the unloaded rotor-bearing system. A 3.25 mil inner clearance is assumed while maintaining the same outer clearance and floating ring mass shown in Table 2. To support these assumptions, an inner diameter of 1.325 in and an outer diameter of 1.785 in for the floating ring, and a bearing diameter of 1.7965 in were selected. Figure 12 suggests the change in radial bearing clearance results in a marginal improvement in the overall thermal stability of the system. However, this improvement is of little practical importance as both bearing configurations are expected to remain stable in this application. Theoretically, though, these results suggest that increasing clearance may reduce thermal unbalance in an unstable floating ring bearing configuration.

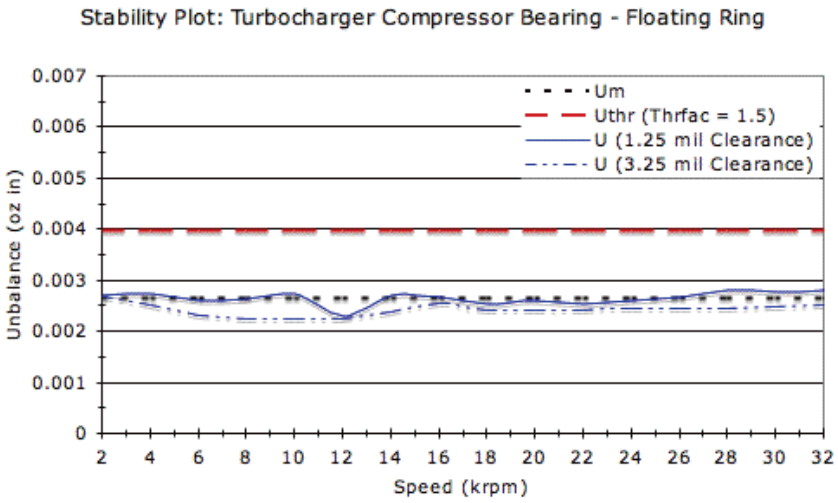

Figure 12: Thermal Stability Plot: Turbocharger with Unloaded Floating Ring Bearings (3.25 mil Inner Clearance)

The aerodynamic load presented in eq (11) was then applied to the rotor-bearing system assuming the original floating ring bearing configuration shown in Figure 7 and Table 2. The log decrement values shown in Figure 13 indicate an improvement in the lateral stability of this loaded configuration when compared to the unloaded version but that the rotor-bearing configuration is expected to remain unstable over the full operating range. However, it is common for high-speed turbochargers with floating ring bearings to operate with marginally unstable bearings where non-linear effects in the rotor-bearing system limit whirl motion preventing bearing failure [26].

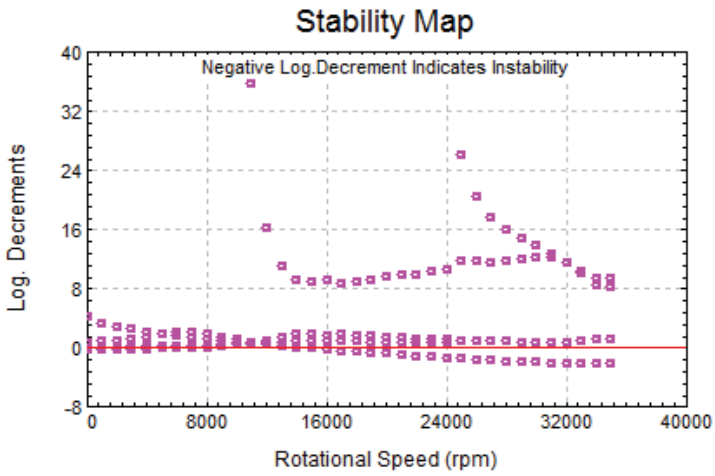

Figure 13: Lateral Stability Map for Floating Ring Bearings with Aero Load

Finally, thermal stability of the rotor-bearing system was considered with aerodynamic loading. Figure 14 shows the calculated unbalance for the unloaded and loaded bearing configurations indicating little change. The upper dashed line at 0.004 oz-in in this plot represents the thermal instability threshold while the lower dashed line at 0.003 oz-in represents the initial mechanical unbalance. Note that Figure 14 reflects the unbalance within the anticipated operating range without showing effects during start-up as was shown in earlier plots; aerodynamic loading outside this range is unknown.

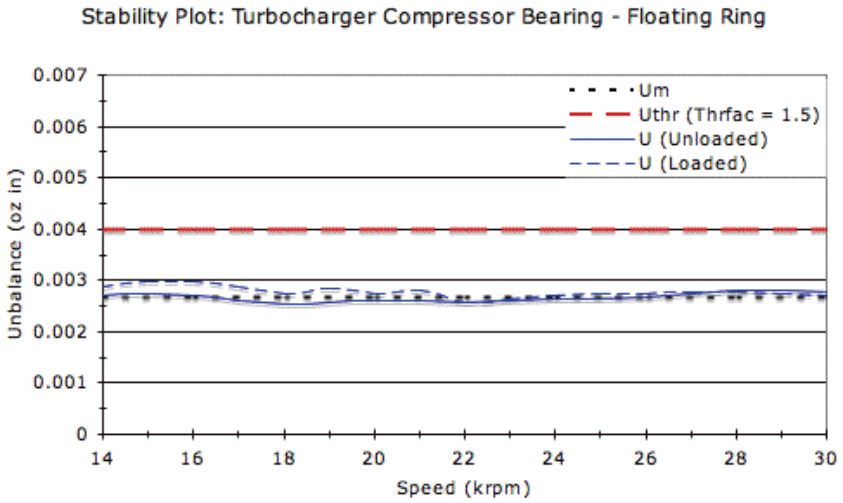

Figure 14: Thermal Stability Plot: Turbocharger with Loaded Floating Ring Bearings (1.25 mil Inner Clearance)

5.2. Turbocharger with Tilting-Pad Journal Bearings

Tilting Pad Journal Bearings consist of varying number of pads set inside a bearing housing. The journal then rides on a fluid film that forms on the pads. Each pad is supported within the housing by a point that allows the pad to rotate in one or more dimensions to better align itself with the journal both to correct for static misalignment of the bearing and rotor and to correct for movement of the shaft.

Tilting pad bearings are more expensive to produce than floating ring bearings and require a larger bearing housing, but their design is inherently more reliable and far more tolerant of rotor-bearing misalignment. In larger turbochargers typical of industrial applications, where downtime for maintenance and repair is very costly, size and acquisition cost become less important than reliability making this style of bearing attractive.

The modeled bearing assumes 4 identical pads as pictured in Figure 15 and detailed Table 3:

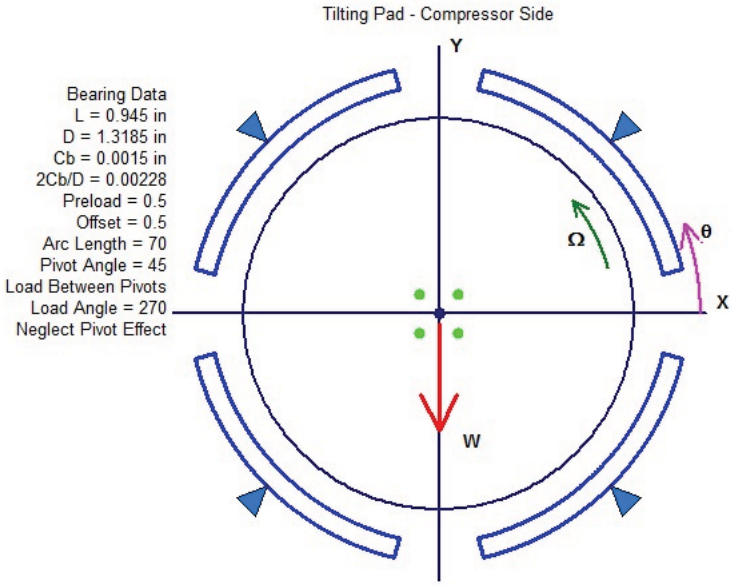

Figure 15: Tilting Pad Journal Bearing Model

Table 3: Bearing Characteristics: Tilting Pad Journal Bearings

Bearing Property		Compressor	Turbine
Journal Radius (in)	R_j	1.3815	1.6925
Bearing Length (in)	L	0.945	0.985
Radial Clearance (mil)	C_b	1.500	1.500
Heat Transfer Coefficient ($HP/in^2/^oF$)	H	$2.435*10^{-6}$	$2.435*10^{-6}$
Journal Coefficient of Thermal Expansion (/ ^oF)	α	$6.11*10^{-6}$	$6.11*10^{-6}$
Gravity Load on Bearing (lb_f)	W_b	27.868	14. 640

A four-pad bearing was selected because the bearing's stiffness and damping characteristics are higher than otherwise identical three, five, or six pad bearings. The pads were then aligned such that the bearing load would pass between the pivots resulting in superior pressure field development, and therefore higher load capacity, than a bearing where the load passes through a pad [27]. Finally, the 1.500 mil radial clearance was selected to maximize the similarities with the floating ring bearing model.

A lateral rotordynamic analysis of this bearing configuration prior to application of the aerodynamic load suggests that it will be stable throughout the entire operating range as shown by the plot of the log decrement versus rotor speed shown in Figure 16. Again, it should be noted that this unloaded condition is a theoretical situation that would not be possible during operation of an actual turbocharger.

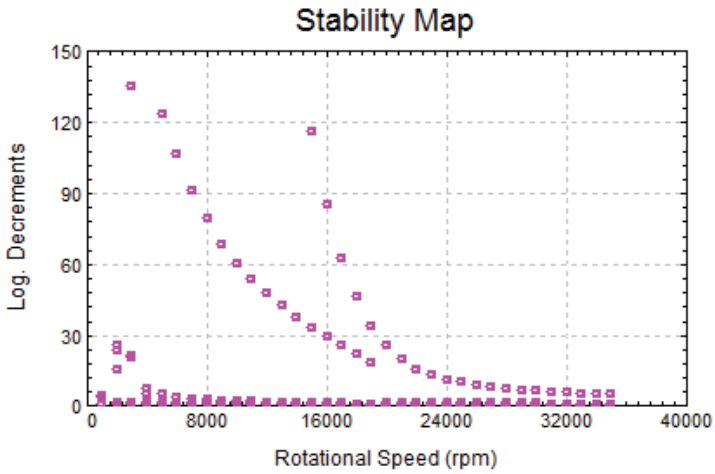

Figure 16: Lateral Stability Map for Tilting Pad Bearing Configuration (1.5 mil Clearance)

A lateral critical speed analysis of the rotor-bearing system indicates that the turbocharger will operate between the second and third critical speeds but that the second mode will likely fall near the lower boundary (14,000 rpm) of the normal operating range. The three curves rising from the left reflect the first three modes versus bearing stiffness while the line in the center of the plot reflects the average direct stiffness (Kxx+Kyy)/2 of the compressor end bearing. The horizontal dashed lines at 14,000 and 30,000 rpm reflect the anticipated upper and lower operating limits of the turbocharger.

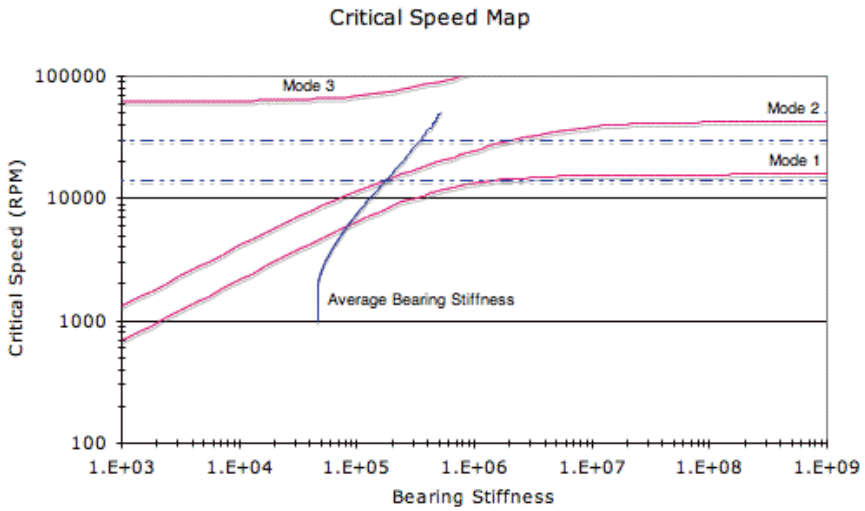

Figure 17: Critical Speed Map - Turbocharger with Tilting Pad Bearings (1.5mil Clearance)

A waterfall plot depicting the response spectra at various speeds, Figure 18, indicates a significant synchronous (1x) response suggesting that thermal instability may be an issue for this configuration over much of the turbocharger's operating range.

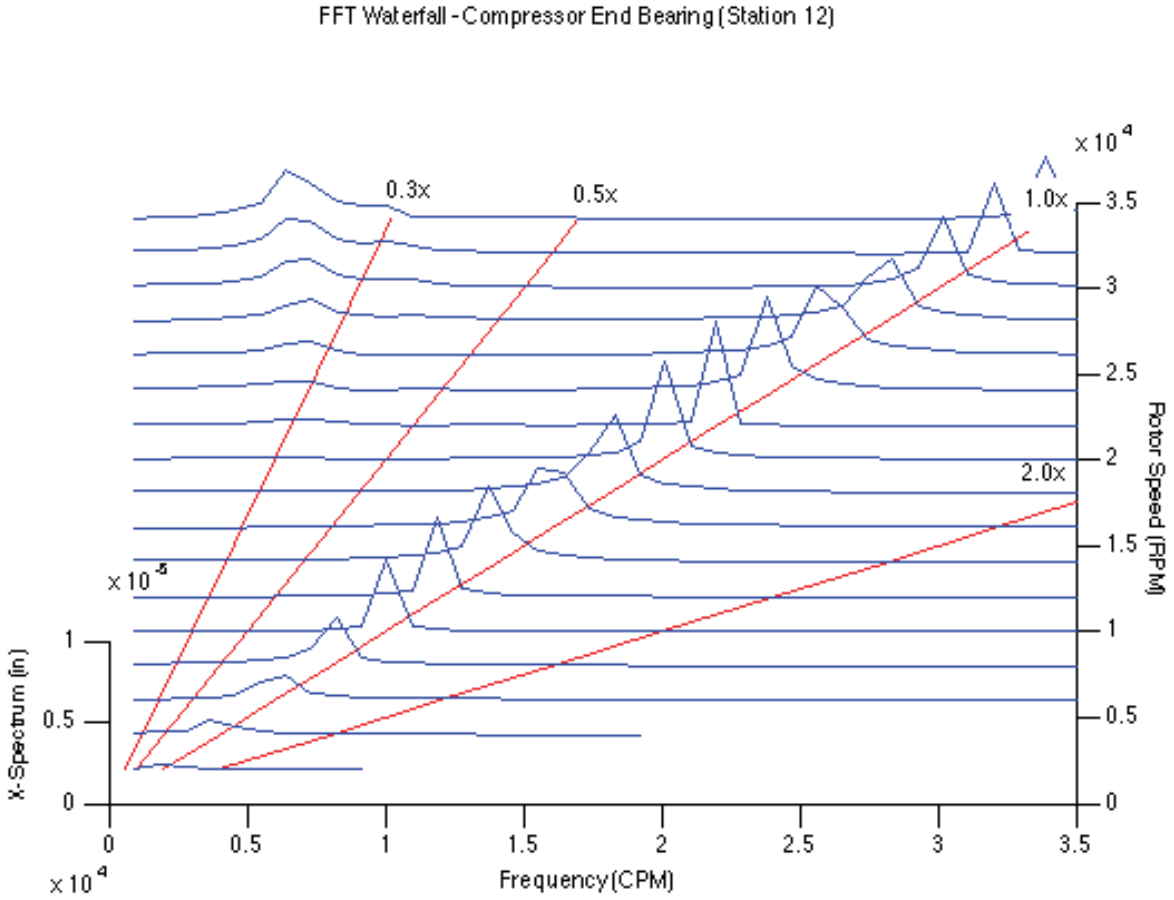

Figure 18: Waterfall Plot: Turbocharger with Unloaded Tilting Pad Bearings (Y-dimension at Station 12)

A thermal unbalance analysis, as shown in Figure 19, confirms those preliminary findings indicating that this bearing configuration will exhibit the Morton Effect at speeds above 6,800 rpm.

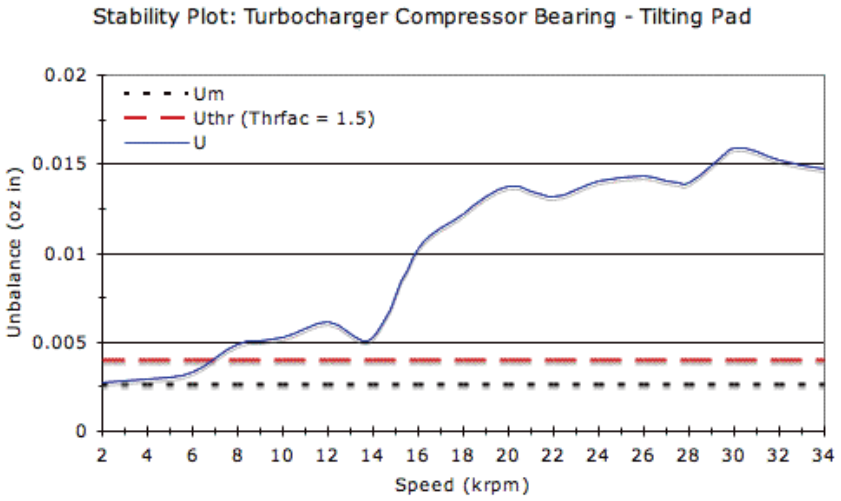

Figure 19: Thermal Stability Plot: Turbocharger with Unloaded Tilting Pad Bearings (1.5mil Clearance)

Increasing the bearing clearance will result in significant improvement to the thermal instability of this rotor-bearing configuration. Analysis of 2.5 mil, 3.5 mil, and 5.0 mil radial clearance configurations show improvement in thermal stability between the 1.5 mil and 3.5 mil radial clearance bearings but increasing to 5.0 mils has a negligible effect. In this rotor-bearing system, the 2.5 or 3.5 mil radial clearances would be appropriate from a thermal instability perspective as both are expected to remain stable over the entire operating range of the turbocharger, but that a 3.0 or 3.5 mil radial clearance would increase the safety margin between the operating range and the stability threshold. Figure 20 depicts the results of this thermal instability analysis showing marked improvement over the operating range when compared to the 1.5 mil radial clearance results.

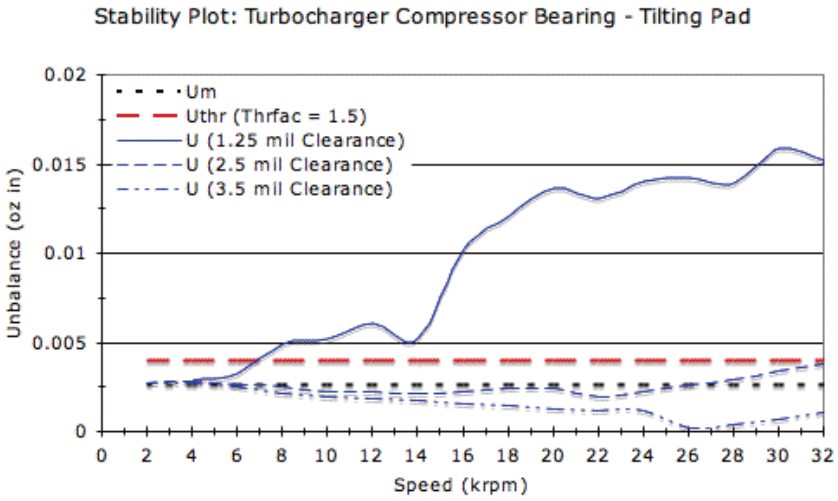

Figure 20: Thermal Stability Plot: Turbocharger with Unloaded Tilting Pad Bearings (3.5mil Clearance)

The new tilting pad bearing configuration with 3.5 mil radial clearance is expected to remain stable from a lateral stability perspective as well, as shown in the Stability Map in Figure 21.

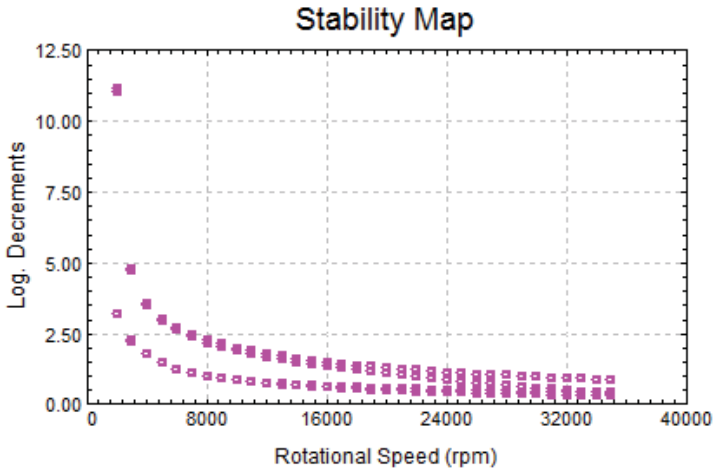

Figure 21: Lateral Stability Map for Tilting Pad Bearing Configuration (3.5 mil Clearance)

The aerodynamic load presented in eq (11) was then applied to the rotor-bearing system assuming the original tilting pad bearing configuration shown in Figure 15 and Table 3. Little effect on the lateral stability of the bearing system as a result of this loading was found within the

normal operational range. As shown in Figure 22, the positive log decrement values indicate the configuration is expected to remain stable over the entire operating range, as was the case in the unloaded configuration.

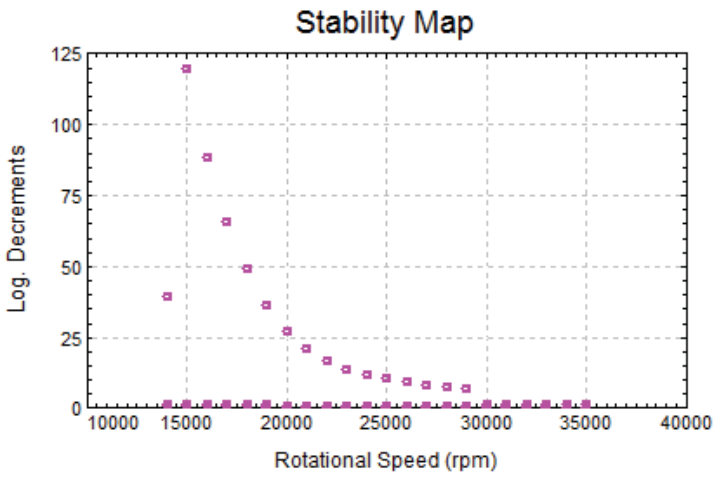

Figure 22: Lateral Stability Map for Loaded Tilting Pad Bearing Configuration

Analysis of the thermal stability of the tilting pad bearing supported system also suggests very limited change in the stability of the loaded and unloaded configurations except in the vicinity of the critical speed. Figure 23 shows the results of the thermal instability analysis for a tilting pad bearing with 1.5 mil radial clearance after considering aerodynamic forces.

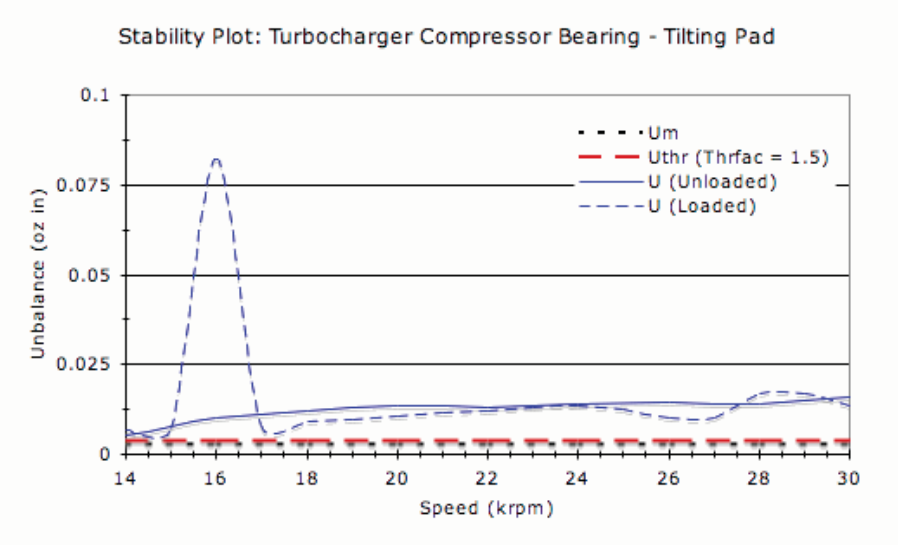

Figure 23: Thermal Stability Plot: Turbocharger with Loaded Tilting Pad Journal Bearings (1.5 mil Clearance)

As in the unloaded configuration, this aerodynamically loaded rotor-bearing system is expected to exhibit the Morton Effect over the entire operating range. In contrast to the unloaded configuration, however, a strong peak in thermal unbalance occurs between 15,000 and 17,000 rpm. A second look at the critical speed map for the system that considers the aerodynamic loading as a static load applied at the center of mass of the compressor wheel indicates that the loading causes the first and second modes to rise such that the second mode occurs at 15,750 rpm as shown in Figure 24.

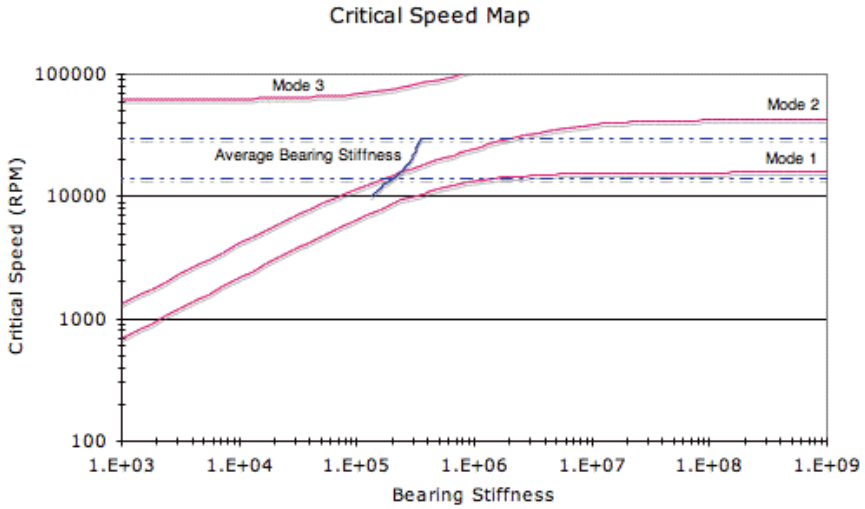

Figure 24: Critical Speed Map - Turbocharger with Loaded Tilting Pad Bearings (1.5mil Clearance)

A Fast Fourier Transform (FFT) Spectrum Analysis of the rotor-bearing system at 15,750 rpm, as depicted in Figure 25, indicates a strong synchronous component of the response that causes the peak seen in Figure 23.

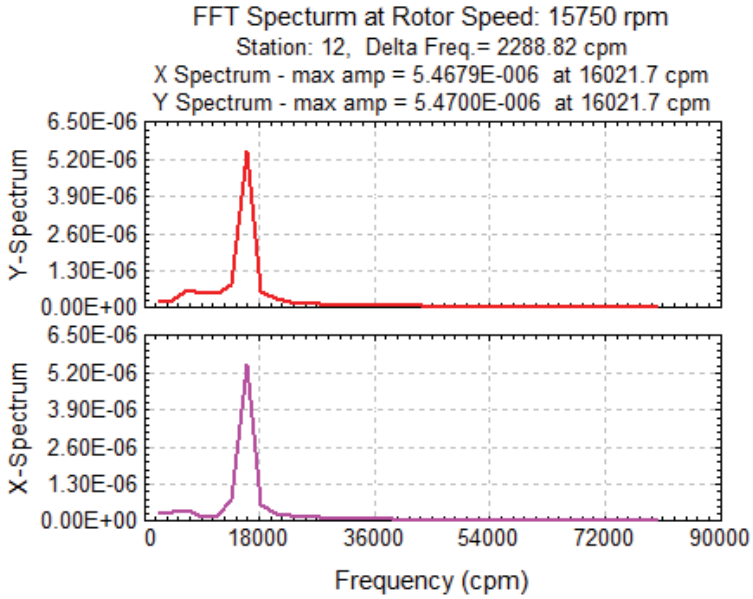

Figure 25: FFT Spectrum Analysis - Turbocharger with Tilting Pad Bearings (1.25 mil Clearance) at Compressor End Bearing

Similar results are found in the tilting pad bearing configuration with the larger 3.5 mil radial clearance when aerodynamic loads are applied. Figure 26 shows a similar spike in thermal instability to that found in the 1.5 mil radial clearance configuration, resulting in development of thermal instability between 15,200 and 16,700 rpm, but the 3.5 mil configuration is expected to remain stable over the remainder of the operating range.

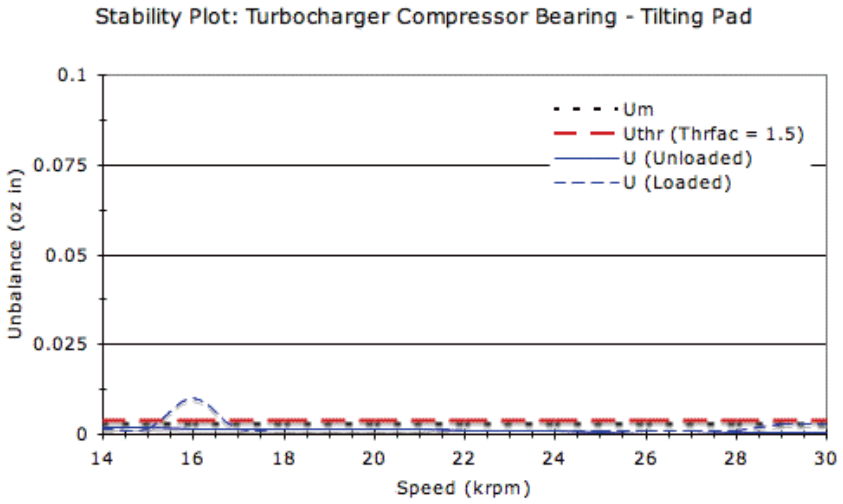

Figure 26: Thermal Stability Plot: Turbocharger with Loaded Tilting Pad Journal Bearings (3.5 mil Clearance)

It should be noted that calculations of bearing stiffness and damping were completed while neglecting the mass of the individual pads. If the pad mass or friction between the pad and its supporting pivot are considered, cross-coupled stiffness develops. However, application of geometric pre-load as was assumed in this analysis results in a stable bearing for typical pad mass values [27].

6. Conclusions

Analytical analysis of floating ring journal bearings and tilting pad journal bearings was performed to consider factors influencing formation of the Morton Effect. Bearing clearance was found to be a critical design factor in tilting pad journal bearings but not in floating ring bearings. Aerodynamic forces resulting from interaction between air exiting a centrifugal compressor and the compressor's volute were also examined and but attempts to correlate the loading with changes in thermal unbalance were inconclusive.

6.1. Bearing Clearance

There is a strong and significant correlation between bearing clearance and the onset and severity of the Morton Effect in tilting pad journal bearings. The results of this analysis, as summarized in Table 4, suggest that thermal stability of the rotor-bearing system will improve as bearing clearance increases to a certain point and then remain constant. Results also indicate that the improvement may be sufficient to allow for stable operation of an otherwise identical and thermally unstable rotor-bearing system. Accordingly, the Morton Effect should be considered when designing such bearings. Furthermore, increasing the bearing clearance in an existing rotor-bearing system may allow for correction of a thermally unstable machine.

Table 4: Summary of Bearing Clearance Results

Clearance	Threshold of Instability	Maximum Total Unbalance
Unloaded Floating Ring Bearings (1.25 mil Radial Inner Clearance)	Stable	0.00275 oz in @ 4,000 rpm
Unloaded Floating Ring Bearings (3.25 mil Radial Inner Clearance)	Stable	0.00269 oz in @ 2,000 rpm
Unloaded Tilting Pad Bearings (1.50 mil Radial Clearance)	6,900 rpm	0.0159 oz in @ 30,000 rpm
Unloaded Tilting Pad Bearings (2.50 mil Radial Clearance)	32,000 rpm	0.00355 oz in @ 30,000 rpm
Unloaded Tilting Pad Bearings (3.50 mil Radial Clearance)	Stable	0.00276 oz in @ 4,000 rpm

Bearing clearance in floating ring bearings appears to have far less influence on the formation of the Morton Effect. While the data suggests that increasing the bearing clearance will result in reduced thermal unbalance, rather large changes in bearing clearance resulted in very small changes. As a result, the Morton Effect is of little concern when selecting bearing clearance in floating ring bearings allowing use of tighter clearances to minimize oil whirl and associated sub-synchronous vibrations.

6.2. Aerodynamic Loading

Aerodynamic loading resulting from the interaction of air exiting a centrifugal compressor wheel and the compressor's volute has little effect on the formation of the Morton Effect. Table 5 reflects the region of unstable operation for each configuration examined based on an analysis conducted between 14,000 and 30,000 rpm.

Table 5: Summary of Aerodynamic Loading Results

Clearance	Unloaded Region of Instability	Loaded Region of Instability
Floating Ring Bearings (1.25 mil Radial Inner Clearance)	Stable	Stable
Floating Ring Bearings (3.25 mil Radial Inner Clearance)	Stable	Stable
Tilting Pad Bearings (1.50 mil Radial Clearance)	14,000 – 30,000 rpm	14,000 – 30,000 rpm
Tilting Pad Bearings (2.50 mil Radial Clearance)	Stable	15,200 – 16,700 rpm, 27,500 – 30,000 rpm
Tilting Pad Bearings (3.50 mil Radial Clearance)	Stable	15,200 – 16,700 rpm

The aerodynamic loading was found to cause the critical modes to rise in speed such that the second mode would shift from approximately 14,000 rpm to 15,750 rpm, falling within the 14,000 rpm to 30,000 rpm operating range. The second mode then excited the thermal instability. It isn't clear, though, if these results are the product of the modeling methodology which employed a static load to approximate the aerodynamic load or is indicative of an actual phenomenon.

The results also indicate that as the bearing clearance increases the level of expected thermal unbalance near the second mode. As a result, it is likely that normal design practices including use safe margins around critical speeds will be adequate to ensure aerodynamic loading does not contribute to thermal instabilities.

6.3. Recommendations

For this particular turbocharger's rotor, either a floating ring bearing with a 1.25 mil inner clearance or a tilting pad bearing with a 3.5 mil clearance would be suitable from a thermal unbalance perspective. Neither configuration is expected to exhibit the Morton Effect within the

expected operating range. While the lateral stability of the tilting pad configuration makes it a superior choice, cost and bearing size could drive selection of the smaller and less expensive floating ring bearing configuration.

7. Summary

Development of orbital or spiral motions of a rotor in a rotor-bearing system is the result of external and self-excitation. When all other variables are held constant, it becomes clear that alterations to bearing geometry have a direct impact on the orbit of the journal within the bearing and therefore the onset of thermal instabilities such as the Morton Effect. This analysis also suggests a possible correlation between aerodynamically induced bearing loads and onset of the Morton Effect within a given rotor-bearing system's normal operating range.

Further refinement of the aerodynamic model is recommended. While the assumed loading used in this analysis is representative of what may be found in an actual marine turbocharger, the direction of the aerodynamic force vector is assumed to be constant. In reality, the direction of this force may shift more than 180 degrees depending on compressor wheel and volute design. This shift in load direction will load the bearings differently than assumed resulting in changes in the bearing stiffness, particularly for tilting pad bearings or fixed bearings such as elliptical bearings. After considering the impact of an aerodynamic load with varying direction, experimental confirmation of the analytical results is recommended.

In addition to the impacts of aerodynamic forces, examination of the impacts of a ship's pitch and roll, as a source of external excitation on the gyroscopics of the turbocharger, are recommended. A ship's movement, particularly in heavier sea states or shock loading caused by pounding waves or icebreaking, would likely present significant and highly variable loads on the rotor-bearing system. Such analysis has the potential to provide insight into design improvements for railroad and automotive applications where motion of the vehicle also presents irregular loading on installed turbochargers.

8. References

[1] Rankine, W. J. M., 1869, "On the Centrifugal Force of Rotating Shafts," The Engineer, **27**, p. 249.
[2] Dunkerley, S., 1894, "On the Whirling and Vibration of Shafts," Philosophical Transactions of the Royal Society of London, **185**(1894), pp. 279-360.
[3] Nelson, F. C., 2003, "A Brief History of Early Rotor Dynamics," Sound and Vibration, **37**(6), pp. 8-11.
[4] Nicholas, J. C., 1994, "Stabilizing Turbomachinery with Pressure Dam Bearings," Encyclopedia of Fluid Mechanics, Gulf, Houston.
[5] Cameron, A., 1966, *The Principles of Lubrication*, Longmans, London.
[6] Reynolds, O., 1886, "On the Theory of Lubrication and Its Application to Mr. Beauchamp Tower's Experiments, Including an Experimental Determination of the Viscosity of Olive Oil," Philosophical Transactions of the Royal Society of London, **177**, pp. 157-234.
[7] Newkirk, B. L., 1924, "Shaft Whipping," General Electric review, **27**(3), p. 169.
[8] Dimarogonas, A. D., 1974, "A Study of the Newkirk Effect in Turbomachinery," Wear, **28**(3), pp. 369-382.
[9] Kellenberger, W., 1980, "Spiral Vibrations Due to the Seal Rings in Turbogenerators Thermally Induced Interaction Between Rotor and Stator," ASME J. Mech. Des., **102**, pp. 177-184.
[10] Schmied, J., "Spiral Vibrations of Rotors," Proc. 11th Biennial ASME Design Engineering Div. Conf., Vib. Noise, DE-VOL 2, Rotating Machinery Dynamics, A. Muszynska, and J. C. Simonis, eds., ASME, pp. 449-456.
[11] de Jongh, F. M., "The Synchronous Rotor Instabiity Phenomenon - Morton Effect," Proc. The Thirty-Seventh Turbomachinery Symposium.
[12] Keogh, P. S., and Morton, P. G., 1993, "Journal Bearing Differential Heating Evaluation with Influence on Rotor Dynamic Behaviour," Proc. Royal Society of London. Series A: Mathematical and Physical Sciences, **441**(1913), pp. 527-548.
[13] Keogh, P. S., and Morton, P. G., 1994, "The Dynamic Nature of Rotor Thermal Bending Due to Unsteady Lubricant Shearing within a Bearing," Proc. Royal Society of London. Series A: Mathematical and Physical Sciences, **445**(1924), pp. 273-290.
[14] Balbahadur, A. C., 2001, "A Thermoelastohydrodynamic Model of the Morton Effect Operating in Overhung Rotors Supported by Plain or Tilting Pad Journal Bearings," Ph.D. Dissertation, Virginia Tech, Blacksburg, VA.
[15] Guo, Z., 2011, "Morton Effect Induced Instability in Mid-Span Rotor-Hydrodynamic Bearing Systems," Ph.D. Dissertation, Virginia Polytechnic Institute and State University, Blacksburg, VA.
[16] Guo, Z. L., and Kirk, R. G., 2011, "Morton Effect Induced Synchronous Instability in Mid-Span Rotor-Bearing Systems-Part I: Mechanism Study," ASME J. Vibration and Acoustics, **133**(6), p. 061004.
[17] Guo, Z. L., and Kirk, R. G., 2011, "Morton Effect Induced Synchronous Instability in Mid-Span Rotor-Bearing Systems, Part 2: Models and Simulations," ASME J. Vibration and Acoustics, **133**(6), p. 061006.
[18] Kirk, R. G., Balbahadur, A. C., and Guo, Z., 2011, "Morton Analysis Program (VT-MAP 5.0) [Software]," Virginia Tech, Blacksburg, VA.

[19] Balbahadur, A. C., and Kirk, R. G., 2004, "Part I - Theoretical Model for a Synchonous Thermal Instability Operating in Overhung Rotors," International Journal of Rotating Machinery, **10**(6), pp. 469-475.
[20] 1979, "Axial and Centrifugal Compressors and Expander-compressors for Petroleum, Chemical and Gas Industry Services," API Standard 617, American Petroleum Institute, Washington, D.C.
[21] Stepanoff, A. J., 1957, *Centrifugal and Axial Flow Pumps: Theory, Design and Application*, Krieder, Malabar, FL.
[22] Chen, W. J., 2009, "DyRoBeS [Software]," Eigen Technologies, Inc.
[23] Watson, N., and Janota, M. S., 1982, *Turbocharging the Internal Combustion Engine*, Wiley, New York.
[24] 2011, "MATLAB R2011 [Software]," Mathworks, Inc.
[25] Alsaeed, A. A., 2005, "Dynamic Stability Evaluation of an Automotive Turbocharger Rotor-Bearing System," M.S. Thesis, Virginia Polytechnic Institute and State University, Blacksburg, VA.
[26] Gunter, E. J., and Chen, W. J., 2005, "Dynamic Analysis of a Turbocharger in Floating Bushing Bearings," ISCORMA-3Cleveland, OH.
[27] Frene, J., Nicolas, D., Deguerce, B., Berthe, D., and Godet, M., 1997, *Hydrodynamic lubrication : Bearings and Thrust Bearings*, Elsevier, Amsterdam [Netherlands]; New York.
[28] Greenhill, A. G., and Cornejo, G. A., 1995, "Critical Speeds Resulting from Unbalance Excitation of Backward Whirl Modes," 1995 Design Engineering Technical Conferences, ASME, pp. 991-1000.
[29] Stokes, G. G., 1844, "On the Theories of the Internal Friction of Fluids in Motion, and of the Equilibrium and Motion of Elastic Solids," Transactions of the Cambridge Philosophical Society, **8**, pp. 287-319.

Appendix A: Turbocharger Model

Used with permission of W. J. Chen.

```
DyRoBeS-Rotor Ver 13.00, W. J. Chen, All Rights Reserved.

   Time: 02:05:49.09 pm   Date: 05-03-2012

   FileName: C:\Turbocharger - EE\Floating\5m_NA\TurboRotor_FR.rot

                    ************************************
                    **            Summary             **
                    **              of                **
                    **           input data           **
                    **              and               **
                    **        system parameters       **
                    ************************************

                        ***** Unit System = 2 *****

                   Engineering English Units (s, in, Lbf, Lbm)

                        ***** Analysis Required *****

                              Model Summary

 *************************** System Parameters ********************************

                             1  Shafts
                            31  Elements
                            73  SubElements
                             7  Materials
                             2  Unbalances
                                2  Mass Unbalances (mew^2)
                             4  Rigid Disks (4 dof)
                             0  Flexible Disks (6 dof)

                             2  Linear Bearings
                             0  NonLinear Bearings
                             0  Flexible Supports

                             0  Axial Loads
                             0  Static Loads
                             0  Time Forcing Functions
                             0  S.S. Harmonic Excitation

                             0  Natural Boundary Conditions
                             0  Geometric Boundary Conditions
                             0  Constraints

                            32  Stations
                           128  Degrees of Freedom

 ******************************************************************************

 *************************** Description Headers *****************************

  Turbocharger with Floating Ring (Bushing) Jounal Bearings

 ******************************************************************************
```

********** Material Properties **********

Property no	Mass Density (Lbm/in^3)	Elastic Modulus (Lbf/in^2)	Shear Modulus (Lbf/in^2)
1	.28400	.29000E+08	.11154E+08
2	.10000E-08	.29000E+08	.11154E+08
3	.97000E-01	.11000E+08	.38000E+07
4	.10000E-08	.11000E+08	.38000E+07
5	.10000E-08	.11000E+08	.38000E+07
6	.97000E-01	.11000E+08	.38000E+07
7	.28300	.29000E+08	.11154E+08

****

********** Shaft Elements **********

Ele no	Sub Ele no	Left End Loc	Length (in)	Mass Inner Diameter (in)	Mass Outer Diameter (in)	Stiffness Inner Diameter (in)	Stiffness Outer Diameter (in)	Material no
1								
	1	.000	.4370	.0000	.9740	.0000	.9740	5
	-2	.437	.1880	.0000	.9740	.0000	2.6320	5
	-3	.625	.2520	.0000	2.6320	.0000	3.3540	5
2								
	1	.877	.3000	1.2500	1.7500	1.2500	1.7500	5
			--------	1.7500	2.2840	1.7500	2.2840	1
			--------	2.6320	3.3540	3.2500	3.6750	5
3								
	1	1.177	.1050	1.2500	1.7500	1.2500	1.7500	5
			--------	1.7500	2.2840	1.7500	2.2840	1
			--------	3.2500	3.6750	3.3400	3.7500	5
	2	1.282	.0320	1.2500	1.7500	1.2500	1.7500	5
			--------	1.7500	2.2840	1.7500	2.3650	1
			--------	3.3400	3.7500	3.3540	3.7750	5
	3	1.314	.5630	1.2500	1.7500	1.2500	1.7500	5
			--------	1.7500	2.3650	1.7500	2.3650	1
			--------	3.3540	3.7750	3.6600	3.9960	5
	4	1.877	.0620	1.7980	2.3650	1.7980	2.3650	1
			--------	3.6600	3.9960	3.6600	3.9960	5
	5	1.939	.4380	1.7980	2.3650	1.7980	2.3650	1
			--------	2.3650	8.1560	2.3650	8.1560	4
	-6	2.377	.0320	1.7980	2.3650	1.7980	2.2880	1
			--------	2.3650	8.1590	2.2880	8.1590	4
4								
	1	2.409	1.2700	1.7980	2.2880	1.7980	2.2880	1
			--------	2.2880	8.1590	2.2880	8.1590	4
5								
	1	3.679	.1040	1.7980	2.2880	1.7980	2.2880	1
			--------	2.2880	8.1590	2.2880	8.1590	4
	-2	3.783	.0320	1.7980	2.2880	1.7980	2.3840	1
			--------	2.2880	8.1590	2.3840	8.1590	4
	3	3.815	.3960	1.7980	2.3840	1.7980	2.3840	1
			--------	2.3840	8.1590	2.3840	9.0135	4
6								
	-1	4.211	.1660	1.7980	2.3500	1.7980	2.4440	1
			--------	2.3500	9.0135	2.4440	9.4420	4
	2	4.377	.0950	.0000	.7500	.0000	.7500	6
			--------	1.7980	2.4440	1.7980	2.4440	1
			--------	2.4440	9.4420	2.4440	9.6565	4

3	4.472	.1500	.0000	1.5000	.0000	1.5000	6
		--------	1.7980	2.4440	1.7980	2.4440	1
		--------	2.4440	9.6565	2.4440	9.8710	4
7							
1	4.622	.1630	.0000	.7040	.0000	.7040	6
		--------	.7040	1.1400	.7040	1.1400	1
		--------	1.2900	2.4440	1.2900	2.4440	1
		--------	2.4440	9.8710	2.4440	10.5480	4
2	4.785	.1500	.0000	.7040	.0000	.7040	6
		--------	.7040	1.1400	.7040	1.1400	1
		--------	1.2900	2.4440	1.2900	2.2880	1
		--------	2.4440	10.5480	2.2880	11.0000	4
3	4.935	.1000	.0000	.7040	.0000	.7040	6
		--------	.7040	1.1400	.7040	1.1400	1
		--------	1.2900	2.0920	1.2900	2.0920	1
		--------	2.0920	11.0000	2.0920	11.5860	4
4	5.035	.3750	.0000	.7040	.0000	.7040	6
		--------	.7040	1.1400	.7040	1.1400	1
		--------	1.2900	2.0920	1.2900	2.0920	1
		--------	2.0920	11.5860	2.0920	11.5860	4
5	5.410	.9520	.0000	.7040	.0000	.7040	6
		--------	.7040	1.2900	.7040	1.3010	1
		--------	1.2900	2.0920	1.3010	2.0920	1
		--------	2.0920	11.5860	2.0920	11.5860	4
8							
1	6.362	.3500	.0000	.7040	.0000	.7040	6
		--------	.7040	1.3010	.7040	1.3030	1
		--------	1.3010	2.0920	1.3030	2.0920	1
		--------	2.0920	11.5860	2.0920	11.5860	4
-2	6.712	.1030	.0000	1.3030	.0000	1.3040	1
		--------	1.3030	2.0920	1.3040	2.0920	1
		--------	2.0920	11.5860	2.0920	11.5860	4
-3	6.815	.3920	.0000	1.3040	.0000	1.3078	1
		--------	1.3040	2.4620	1.3078	2.4620	1
		--------	2.4620	8.0680	2.4620	3.1260	4
-4	7.207	.0240	.0000	1.3078	.0000	1.3080	1
		--------	1.3078	2.7880	1.3080	2.7880	1
5	7.231	.0990	.0000	1.2500	.0000	1.2500	1
		--------	1.2900	2.7880	1.2900	2.7880	1
6	7.330	.0370	.0000	1.2500	.0000	1.2500	1
		--------	1.2900	1.8490	1.2900	1.8490	1
9							
1	7.367	.3480	.0000	1.3080	.0000	1.3080	1
		--------	1.2900	1.8490	1.2900	1.8490	1
2	7.715	.0315	.0000	1.3080	.0000	1.3080	1
		--------	1.2900	1.6560	1.2900	1.6560	1
3	7.747	.2025	.0000	1.2840	.0000	1.2840	1
		--------	1.2900	1.8490	1.2900	1.8490	1
4	7.949	.0390	.0000	1.2840	.0000	1.2840	1
		--------	1.2900	1.6560	1.2900	1.6560	1
5	7.988	.0710	.0000	1.2840	.0000	1.2840	1
		--------	1.2900	1.8490	1.2900	1.8490	1
6	8.059	.0390	.0000	1.2840	.0000	1.2840	1
		--------	1.2900	1.6560	1.2900	1.6560	1
7	8.098	.1420	.0000	1.2840	.0000	1.2840	1
		--------	1.2900	1.8490	1.2900	1.8490	1
8	8.240	.2770	.0000	1.2840	.0000	1.2840	1
		--------	1.2900	1.5000	1.2900	1.8260	1
10							
1	8.517	.1120	.0000	1.2840	.0000	1.2840	1
11							
1	8.629	.7380	.0000	1.3185	.0000	1.3185	1

```
12
    1     9.367     .7380     .0000    1.3185       .0000    1.3185     1
 13
    1    10.105     .1300     .0000    1.2840       .0000    1.2840     1
 14
    1    10.235     .3310     .0000    1.2840       .0000    1.2840     1
                  --------    1.3750    2.8440      1.3750    2.8440     1
 15
    1    10.566     .1690     .0000    1.6180       .0000    1.6180     1
                  --------    1.6630    2.8440      1.6630    2.8440     1
    2    10.735     .4380     .0000    1.6180       .0000    1.6180     1
                  --------    1.6630    2.6880      1.6630    2.6880     1
    3    11.173     .1070     .0000    1.6180       .0000    1.6630     1
                  --------    1.6630    2.0200      1.6630    2.0200     1
   -4    11.280     .1250     .0000    1.6180       .0000    1.6630     1
                  --------    1.6630    2.0200      1.6630    2.0200     1
 16
    1    11.405     .3800     .0000    1.6630       .0000    1.6630     1
                  --------    1.6630    2.0200      1.6630    2.0200     1
    2    11.785     .5260     .0000    1.6160       .0000    1.6160     1
                  --------    1.6630    2.0200      1.6630    2.0200     1
   -3    12.311     .1250     .0000    1.6160       .0000    1.6700     1
                  --------    1.6630    2.0200      1.6630    2.0200     1
    4    12.436     .3800     .0000    1.6700       .0000    1.6700     1
                  --------    1.6630    2.0200      1.6630    2.0200     1
 17
    1    12.816     .0290     .0000    1.6160       .0000    1.6160     1
                  --------    1.6630    2.0200      1.6630    2.0200     1
 18
    1    12.845    2.2610     .0000    1.6160       .0000    1.6160     1
   -2    15.106     .1250     .0000    1.6160       .0000    1.6930     1
 19
    1    15.231     .8555     .0000    1.6930       .0000    1.6930     1
 20
    1    16.087     .8555     .0000    1.6930       .0000    1.6930     1
 21
   -1    16.942     .0500     .0000    1.6930       .0000    1.6550     1
   -2    16.992     .0500     .0000    1.6550       .0000    1.6160     1
    3    17.042     .0500     .0000    1.6160       .0000    1.6160     1
   -4    17.092     .0500     .0000    1.6160       .0000    1.6550     1
   -5    17.142     .0500     .0000    1.6550       .0000    1.6930     1
 22
    1    17.192     .1250     .0000    1.8460       .0000    1.8460     1
 23
   -1    17.317     .0406     .0000    1.8460       .0000    1.8660     1
   -2    17.358     .0406     .0000    1.8660       .0000    1.8860     1
    3    17.398     .0406     .0000    1.8860       .0000    1.8860     1
   -4    17.439     .0406     .0000    1.8860       .0000    1.8660     1
   -5    17.479     .0406     .0000    1.8660       .0000    1.8460     1
 24
    1    17.520     .1250     .0000    1.8460       .0000    1.8460     1
 25
    1    17.645     .1880     .0000    1.4040       .0000    1.4040     1
 26
    1    17.833     .1250     .0000    1.8460       .0000    1.8460     1
 27
   -1    17.958     .1090     .0000    1.8460       .0000    2.1260     1
 28
    1    18.067     .2890     .0000    2.1250       .0000    2.1250     2
 29
    1    18.356     .6000     .0000    2.1250       .0000    2.1250     2
                  --------    2.1250    7.2500      2.1250    7.5000     2
```

```
  30
     1    18.956     .6000     .0000    2.1250       .0000    2.1250     2
                   --------    2.1250    7.5000      2.1250    7.7500     2
  31
     1    19.556     .5000     .0000    2.1875       .0000    2.1875     2

 ***************************************************************************

 ***************************** Rigid/Flexible Disks *****************************
  Stn                      Diametral        Polar       Skew    Skew
   no          Mass         Inertia       Inertia        X       Y     Offset
               (Lbm)      (Lbm-in^2)     (Lbm-in^2)   (deg.)  (deg.)   (in)

   30        15.700        74.600         146.20       .0000   .0000    .1000
    8        9.5100        58.300         111.50       .0000   .0000    .0000
    5        4.2900        15.800         25.000       .0000   .0000    .0000
    3        .48000        .43000         .68000       .0000   .0000    .0000

 ***************************************************************************

 ****************** Rotor Equivalent Rigid Body Properties ******************
  Rotor Left End            C.M.              Diametral     Polar      Speed
   no   Location  Length  Location    Mass     Inertia     Inertia     Ratio
          (in)     (in)     (in)     (Lbm)    (Lbm-in^2)  (Lbm-in^2)

    1      .000    20.056    11.681  42.510      1922.      291.248     1.0000

 ***************************************************************************

 ***************************** Bearing Coefficients *****************************
  StnI,  J   Angle   rpm     ---------------- Coefficients -----------------

   12    0      .00           (Data File:C:\Turbocharger - EE\Floating\5m_NA\Floating
Ring - Compressor.brg
                      Kt: Lbf/in, Ct: Lbf-s/in;  Kr: Lbf-in, Cr: Lbf-in-s

                2000.00
  Kxx  Kxy  Kyx  Kyy    5665.83     -527.625     -14993.9      26877.8
  Cxx  Cxy  Cyx  Cyy    43.1564     -62.0191     -56.0185      342.225
  Krr  Krs  Ksr  Kss    .000000      .000000      .000000      .000000
  Crr  Crs  Csr  Css    .000000      .000000      .000000      .000000
                6000.00
  Kxx  Kxy  Kyx  Kyy    6615.28      306.900     -16008.0      20205.8
  Cxx  Cxy  Cyx  Cyy    26.0051     -31.1210     -29.5011      133.021
  Krr  Krs  Ksr  Kss    .000000      .000000      .000000      .000000
  Crr  Crs  Csr  Css    .000000      .000000      .000000      .000000
                10000.0
  Kxx  Kxy  Kyx  Kyy    6845.50      1098.59     -16445.9      16603.9
  Cxx  Cxy  Cyx  Cyy    20.9082     -21.4635     -20.7257      82.5101
  Krr  Krs  Ksr  Kss    .000000      .000000      .000000      .000000
  Crr  Crs  Csr  Css    .000000      .000000      .000000      .000000
                14000.0
  Kxx  Kxy  Kyx  Kyy    6838.92      2458.85     -16921.4      13497.5
  Cxx  Cxy  Cyx  Cyy    20.1483     -17.9953     -17.5766      61.0973
  Krr  Krs  Ksr  Kss    .000000      .000000      .000000      .000000
  Crr  Crs  Csr  Css    .000000      .000000      .000000      .000000
                18000.0
  Kxx  Kxy  Kyx  Kyy    6429.60      3633.30     -17417.7      10844.0
  Cxx  Cxy  Cyx  Cyy    19.3692     -15.5131     -15.2987      49.1743
  Krr  Krs  Ksr  Kss    .000000      .000000      .000000      .000000
  Crr  Crs  Csr  Css    .000000      .000000      .000000      .000000
```

```
                22000.0
  Kxx  Kxy  Kyx  Kyy    5243.02      4152.62     -17478.0      8685.26
  Cxx  Cxy  Cyx  Cyy    17.2467     -12.4887     -12.4070      40.5623
  Krr  Krs  Ksr  Kss    .000000      .000000      .000000      .000000
  Crr  Crs  Csr  Css    .000000      .000000      .000000      .000000
                26000.0
  Kxx  Kxy  Kyx  Kyy    3598.13      4489.17     -17472.1      6581.47
  Cxx  Cxy  Cyx  Cyy    15.3120     -10.0707     -10.0739      34.5344
  Krr  Krs  Ksr  Kss    .000000      .000000      .000000      .000000
  Crr  Crs  Csr  Css    .000000      .000000      .000000      .000000
                30000.0
  Kxx  Kxy  Kyx  Kyy    2249.01      5753.32     -18068.4      3867.20
  Cxx  Cxy  Cyx  Cyy    15.6173     -9.44295     -9.50008      31.1079
  Krr  Krs  Ksr  Kss    .000000      .000000      .000000      .000000
  Crr  Crs  Csr  Css    .000000      .000000      .000000      .000000
                34000.0
  Kxx  Kxy  Kyx  Kyy    395.844      6647.99     -18536.8      1185.79
  Cxx  Cxy  Cyx  Cyy    15.2660     -8.56516     -8.66746      28.3356
  Krr  Krs  Ksr  Kss    .000000      .000000      .000000      .000000
  Crr  Crs  Csr  Css    .000000      .000000      .000000      .000000

   20    0      .00            (Data File:C:\Turbocharger - EE\Floating\5m_NA\Floating
Ring - Turbine.brg
                      Kt: Lbf/in, Ct: Lbf-s/in;  Kr: Lbf-in, Cr: Lbf-in-s

                2000.00
  Kxx  Kxy  Kyx  Kyy    4572.19      2358.44     -10468.0      8996.69
  Cxx  Cxy  Cyx  Cyy    67.1449     -57.9269     -53.8540      221.554
  Krr  Krs  Ksr  Kss    .000000      .000000      .000000      .000000
  Crr  Crs  Csr  Css    .000000      .000000      .000000      .000000
                6000.00
  Kxx  Kxy  Kyx  Kyy    5334.83      5147.63     -12301.2      6006.96
  Cxx  Cxy  Cyx  Cyy    47.7018     -26.4427     -25.2919      94.7224
  Krr  Krs  Ksr  Kss    .000000      .000000      .000000      .000000
  Crr  Crs  Csr  Css    .000000      .000000      .000000      .000000
                10000.0
  Kxx  Kxy  Kyx  Kyy    5512.30      8820.92     -15031.0      4288.22
  Cxx  Cxy  Cyx  Cyy    47.1649     -19.1475     -18.6585      70.3467
  Krr  Krs  Ksr  Kss    .000000      .000000      .000000      .000000
  Crr  Crs  Csr  Css    .000000      .000000      .000000      .000000
                14000.0
  Kxx  Kxy  Kyx  Kyy    4589.12      10977.6     -17422.8      3171.39
  Cxx  Cxy  Cyx  Cyy    41.6102     -13.1460     -13.0060      59.9688
  Krr  Krs  Ksr  Kss    .000000      .000000      .000000      .000000
  Crr  Crs  Csr  Css    .000000      .000000      .000000      .000000
                18000.0
  Kxx  Kxy  Kyx  Kyy    3603.04      14156.7     -20530.4      1679.03
  Cxx  Cxy  Cyx  Cyy    41.3147     -10.6591     -10.7101      55.3468
  Krr  Krs  Ksr  Kss    .000000      .000000      .000000      .000000
  Crr  Crs  Csr  Css    .000000      .000000      .000000      .000000
                22000.0
  Kxx  Kxy  Kyx  Kyy    2169.39      16982.3     -23688.7      20.8031
  Cxx  Cxy  Cyx  Cyy    40.3377     -8.79678     -8.98780      52.7124
  Krr  Krs  Ksr  Kss    .000000      .000000      .000000      .000000
  Crr  Crs  Csr  Css    .000000      .000000      .000000      .000000
                26000.0
  Kxx  Kxy  Kyx  Kyy    657.050      20631.1     -27275.2     -2058.85
  Cxx  Cxy  Cyx  Cyy    41.2957     -7.89658     -8.20466      51.2705
  Krr  Krs  Ksr  Kss    .000000      .000000      .000000      .000000
  Crr  Crs  Csr  Css    .000000      .000000      .000000      .000000
                30000.0
  Kxx  Kxy  Kyx  Kyy   -1389.80      23505.6     -30658.1     -4279.38
  Cxx  Cxy  Cyx  Cyy    40.6966     -6.89264     -7.29876      50.2162
```

```
 Krr  Krs  Ksr  Kss    .000000      .000000      .000000      .000000
 Crr  Crs  Csr  Css    .000000      .000000      .000000      .000000
                34000.0
 Kxx  Kxy  Kyx  Kyy   -3781.94      26249.3     -34053.5     -6778.03
 Cxx  Cxy  Cyx  Cyy    40.0539     -6.08400     -6.57703      49.4779
 Krr  Krs  Ksr  Kss    .000000      .000000      .000000      .000000
 Crr  Crs  Csr  Css    .000000      .000000      .000000      .000000

*******************************************************************************

************************** Mass Unbalance (M x Ecc) **************************
    Ele   SubEle     ----- Left End -----         ----- Right End -----
     no      no       Magnitude      Angle        Magnitude      Angle
                       (oz-in)      (degree)       (oz-in)      (degree)

     30       1        .26600E-02   270.00          .00000          .00
      7       5        .26600E-02   270.00          .00000          .00

*******************************************************************************

*********************** Gravity Constant (g) (in/s^2) ************************

             X direction =  .000000         Y direction = -386.088

*******************************************************************************

  Time: 02:05:49.82 pm   Date: 05-03-2012
```

Appendix B: Governing Fluid Mechanics Equations

The Navier-Stokes and Reynolds Equations derived in the following sections are the fundamental equations that describe the flow of a fluid in general and the flow of a lubricant in a journal bearing, respectively.

B.1. Navier-Stokes Equations

The Navier-Stokes Equations were developed independently by Claude Louis Marie Navier in 1823 and Sir George Gabriel Stokes [29], providing an elegant yet virtually unsolvable set of three, second-order, non-linear, partial differential equations. When combined with the Continuity Equation (conservation of mass), Conservation of Energy, and the Thermodynamic Equation of State, a complete mathematical description of a fluid flow results. While the non-linear nature of the Navier-Stokes equations limits the situations where an exact solution may be found, experimental results for solvable cases have closely matched experimental results.

The Navier-Stoke's Equations consist of three equations with the unknowns of velocity in three dimensions, pressure, and density, all as functions of position and time. The equations are derived below in their most general form beginning with Newton's Second Law relating the sum of body forces and surface forces to the acceleration of the mass of fluid:

$$\sum F = m\dot{v} \longrightarrow F_{body} + F_{surface} + F_{inertia} = m\dot{v} \qquad (1)$$

Body forces are those external forces acting on the mass of the fluid element such as gravity (g).

$$\partial F_{body} = \partial m \quad g \tag{2}$$

However, to minimize the number of assumptions and in keeping with the work of Stokes and Reynolds, body forces will simply be noted as X, Y, and Z representing the magnitude of the body force vector in the x, y, and z dimensions, on a per unit of mass basis. Thus, eq **(2)** becomes:

$$\partial F_{body} = N_i \rho \partial x \partial y \partial z \tag{3}$$

where N_i is X, Y, or Z for i=1 through 3.

Surface forces account for interaction of the fluid particle with its surroundings, expressed as forces normal to the surface (σ) and forces parallel to the surface (τ).

$$\begin{aligned}
\delta F_x &= \left(\sigma_{xx} + \frac{1}{2}\frac{\partial}{\partial x}\sigma_{xx}\partial x\right)\partial y\partial z - \left(\sigma_{xx} - \frac{1}{2}\frac{\partial}{\partial x}\sigma_{xx}\partial x\right)\partial y\partial z + \left(\tau_{yx} + \frac{1}{2}\frac{\partial}{\partial y}\tau_{yx}\partial y\right)\partial x\partial z \\
&\quad - \left(\tau_{yx} - \frac{1}{2}\frac{\partial}{\partial y}\tau_{yx}\partial y\right)\partial x\partial z + \left(\tau_{zx} + \frac{1}{2}\frac{\partial}{\partial z}\tau_{zx}\partial z\right)\partial x\partial y - \left(\tau_{zx} - \frac{1}{2}\frac{\partial}{\partial z}\tau_{zx}\partial z\right)\partial x\partial y \\
\delta F_x &= \sigma_{xx}\partial y\partial z + \frac{1}{2}\frac{\partial}{\partial x}\sigma_{xx}\partial x\partial y\partial z - \sigma_{xx}\partial y\partial z + \frac{1}{2}\frac{\partial}{\partial x}\sigma_{xx}\partial x\partial y\partial z + \tau_{yx}\partial x\partial z \\
&\quad + \frac{1}{2}\frac{\partial}{\partial y}\tau_{yx}\partial y\partial x\partial z - \tau_{yx}\partial x\partial z + \frac{1}{2}\frac{\partial}{\partial y}\tau_{yx}\partial y\partial x\partial z + \tau_{zx}\partial x\partial y + \frac{1}{2}\frac{\partial}{\partial z}\tau_{zx}\partial z\partial x\partial y \\
&\quad - \tau_{zx}\partial x\partial y + \frac{1}{2}\frac{\partial}{\partial z}\tau_{zx}\partial z\partial x\partial y \\
\delta F_x &= \frac{\partial}{\partial x}\sigma_{xx}\partial x\partial y\partial z + \frac{\partial}{\partial y}\tau_{yx}\partial y\partial x\partial z + \frac{\partial}{\partial z}\tau_{zx}\partial z\partial x\partial y
\end{aligned}$$

$$\delta F_x = \left(\frac{\partial \sigma_{xx}}{\partial x} + \frac{\partial \tau_{yx}}{\partial y} + \frac{\partial \tau_{zx}}{\partial z}\right)\partial x\partial y\partial z \tag{4}$$

Similarly, the net surface forces in the y and z directions are

$$\delta F_y = \left(\frac{\partial \tau_{xx}}{\partial x} + \frac{\partial \sigma_{yy}}{\partial y} + \frac{\partial \tau_{zx}}{\partial z} \right) \partial x \partial y \partial z \qquad (5)$$

$$\delta F_z = \left(\frac{\partial \tau_{xz}}{\partial x} + \frac{\partial \tau_{yz}}{\partial y} + \frac{\partial \sigma_{zz}}{\partial z} \right) \partial x \partial y \partial z \qquad (6)$$

The acceleration of fluid within the control volume is the time rate of change of velocity of the fluid. Beginning with the velocity as a function of position and time and then differentiating using the chain rule provides the acceleration:

$$v(t) = V\left[x(t), y(t), z(t)\right]$$

$$a = \frac{dV}{dt} = \frac{\partial V}{\partial t} + \frac{\partial V}{\partial x}\frac{dx(t)}{dt} + \frac{\partial V}{\partial y}\frac{dy(t)}{dt} + \frac{\partial V}{\partial z}\frac{dz(t)}{dt}$$

$$a = \frac{\partial V}{\partial t} + u\frac{\partial V}{\partial x} + v\frac{\partial V}{\partial y} + w\frac{\partial V}{\partial z} \qquad (7)$$

Substituting the net surface force, eq **(3)**, the net body forces, eq **(4)** and the acceleration terms, eq (7) into the eq **(1)** in the x direction:

$$\delta F_x + \delta F_{body} =$$

$$\left(\frac{\partial \sigma_{xx}}{\partial x} + \frac{\partial \tau_{yx}}{\partial y} + \frac{\partial \tau_{zx}}{\partial z} \right) \partial x \partial y \partial z + X \rho \partial x \partial y \partial z = \left(\rho \partial x \partial y \partial z \right) \left(\frac{\partial V}{\partial t} + u\frac{\partial V}{\partial x} + v\frac{\partial V}{\partial y} + w\frac{\partial V}{\partial z} \right)$$

$$\left(\frac{\partial \sigma_{xx}}{\partial x}+\frac{\partial \tau_{yx}}{\partial y}+\frac{\partial \tau_{zx}}{\partial z}\right)+X\rho=\rho\left(\frac{\partial u}{\partial t}+u\frac{\partial u}{\partial x}+v\frac{\partial u}{\partial y}+w\frac{\partial u}{\partial z}\right) \qquad (8)$$

and similarly in the y and z directions:

$$\left(\frac{\partial \tau_{xy}}{\partial x}+\frac{\partial \sigma_{yy}}{\partial y}+\frac{\partial \tau_{zy}}{\partial z}\right)+Y\rho=\rho\left(\frac{\partial v}{\partial t}+u\frac{\partial v}{\partial x}+v\frac{\partial v}{\partial y}+w\frac{\partial v}{\partial z}\right) \qquad (9)$$

$$\left(\frac{\partial \tau_{xy}}{\partial x}+\frac{\partial \tau_{yz}}{\partial y}+\frac{\partial \sigma_{zz}}{\partial z}\right)+Z\rho=\rho\left(\frac{\partial w}{\partial t}+u\frac{\partial w}{\partial x}+v\frac{\partial w}{\partial y}+w\frac{\partial w}{\partial z}\right) \qquad (10)$$

By definition, a Newtonian fluid has a linear stress-strain relationship. The total stress within the fluid may therefore be described as the sum of the pressure, the stresses associated with expansion of the fluid, and the shear stresses:

$$\sigma_i=-p+\lambda\varepsilon+2\mu\frac{\partial \mu_i}{\partial x_i} \qquad (11)$$

where the dilation, ε, represents the expansion of the fluid:

$$\varepsilon=\left(\frac{\partial u}{\partial x}+\frac{\partial v}{\partial y}+\frac{\partial w}{\partial z}\right) \qquad (12)$$

and λ represents a second viscosity coefficient. The value of this coefficient may be expressed in terms of the absolute viscosity by considering the fluid pressure as an average of the normal stresses and then substituting eq (11) for the stresses resulting in Stoke's Hypothesis:

$$\sigma_x + \sigma_y + \sigma_z = -3p$$

$$\left(-p + \lambda\varepsilon + 2\mu\frac{\partial u}{\partial x}\right) + \left(-p + \lambda\varepsilon + 2\mu\frac{\partial v}{\partial y}\right) + \left(-p + \lambda\varepsilon + 2\mu\frac{\partial w}{\partial z}\right) = -3p$$

$$-3p + 3\lambda\varepsilon + 2\mu\left(\frac{\partial \mu}{\partial x} + \frac{\partial v}{\partial y} + \frac{\partial w}{\partial z}\right) = -3p$$

$$3\lambda\varepsilon + 2\mu\varepsilon = 0$$

$$\lambda = \frac{-2\mu}{3} \qquad (13)$$

Then, introducing Newton's Law of Viscous Friction:

$$\tau_{xy} = \tau_{yx} = \mu\left(\frac{\partial u}{\partial y} + \frac{\partial v}{\partial x}\right) \qquad (14)$$

$$\tau_{xz} = \tau_{zx} = \mu\left(\frac{\partial u}{\partial z} + \frac{\partial w}{\partial x}\right) \qquad (15)$$

$$\tau_{yz} = \tau_{zy} = \mu\left(\frac{\partial v}{\partial z} + \frac{\partial w}{\partial y}\right) \qquad (16)$$

Finally, substituting the equations for shear and normal stresses into the surface forces equations (8) and simplifying results in the Navier-Stokes Equations:

$$\frac{\partial \sigma_{xx}}{\partial x} + \frac{\partial \tau_{yx}}{\partial y} + \frac{\partial \tau_{zx}}{\partial z} + g_x \rho = \rho\left(\frac{\partial u}{\partial t} + u\frac{\partial u}{\partial x} + v\frac{\partial u}{\partial y} + w\frac{\partial u}{\partial z}\right)$$

$$\sigma_i = -p - \frac{2}{3}\mu\left(\frac{\partial u}{\partial x} + \frac{\partial v}{\partial y} + \frac{\partial w}{\partial z}\right) + 2\mu\frac{\partial u}{\partial x}$$

$$\tau_{xy} = \tau_{yx} = \mu\left(\frac{\partial u}{\partial y} + \frac{\partial v}{\partial x}\right)$$

$$\tau_{xz} = \tau_{zx} = \mu\left(\frac{\partial u}{\partial z} + \frac{\partial w}{\partial x}\right)$$

$$\frac{\partial}{\partial x}\left(-p - \frac{2}{3}\mu\left(\frac{\partial u}{\partial x} + \frac{\partial v}{\partial y} + \frac{\partial w}{\partial z}\right) + 2\mu\frac{\partial u}{\partial x}\right) + \frac{\partial}{\partial y}\left(\mu\left(\frac{\partial u}{\partial y} + \frac{\partial v}{\partial x}\right)\right) + \frac{\partial}{\partial z}\mu\left(\frac{\partial u}{\partial z} + \frac{\partial w}{\partial x}\right) + X\rho$$

$$= \rho\left(\frac{\partial u}{\partial t} + u\frac{\partial u}{\partial x} + v\frac{\partial u}{\partial y} + w\frac{\partial u}{\partial z}\right)$$

$$-\frac{\partial p}{\partial x} - \frac{2}{3}\frac{\partial}{\partial x}\mu\left(\frac{\partial u}{\partial x} + \frac{\partial v}{\partial y} + \frac{\partial w}{\partial z}\right) + 2\frac{\partial}{\partial x}\left(\mu\frac{\partial u}{\partial x}\right) + \frac{\partial}{\partial y}\left(\mu\left(\frac{\partial u}{\partial y} + \frac{\partial v}{\partial x}\right)\right) + \frac{\partial}{\partial z}\mu\left(\frac{\partial u}{\partial z} + \frac{\partial w}{\partial x}\right) + X\rho$$

$$= \rho\left(\frac{\partial u}{\partial t} + u\frac{\partial u}{\partial x} + v\frac{\partial u}{\partial y} + w\frac{\partial u}{\partial z}\right)$$

$$-\frac{\partial p}{\partial x} - \frac{2}{3}\frac{\partial}{\partial x}\mu\left(\frac{\partial u}{\partial x} + \frac{\partial v}{\partial y} + \frac{\partial w}{\partial z}\right) + 2\frac{\partial}{\partial x}\left(\mu\frac{\partial u}{\partial x}\right) + \frac{\partial}{\partial y}\left(\mu\left(\frac{\partial u}{\partial y} + \frac{\partial v}{\partial x}\right)\right) + \frac{\partial}{\partial z}\mu\left(\frac{\partial u}{\partial z} + \frac{\partial w}{\partial x}\right) + X\rho$$

$$= \rho\frac{Du}{Dt}$$

$$\rho\frac{Du}{Dt} = -\frac{\partial p}{\partial x} - \frac{2}{3}\frac{\partial}{\partial x}\mu\left(\frac{\partial u}{\partial x} + \frac{\partial v}{\partial y} + \frac{\partial w}{\partial z}\right) + 2\frac{\partial}{\partial x}\left(\mu\frac{\partial u}{\partial x}\right) + \frac{\partial}{\partial y}\left(\mu\left(\frac{\partial u}{\partial y} + \frac{\partial v}{\partial x}\right)\right)$$
$$+ \frac{\partial}{\partial z}\mu\left(\frac{\partial u}{\partial z} + \frac{\partial w}{\partial x}\right) + X\rho \qquad (17)$$

and similarly in the Y and Z dimensions:

$$\rho\frac{Dv}{Dt} = -\frac{\partial p}{\partial y} - \frac{2}{3}\frac{\partial}{\partial y}\mu\left(\frac{\partial u}{\partial x} + \frac{\partial v}{\partial y} + \frac{\partial w}{\partial z}\right) + \frac{\partial}{\partial x}\left(\mu\left(\frac{\partial u}{\partial y} + \frac{\partial v}{\partial x}\right)\right) + 2\frac{\partial}{\partial y}\left(\mu\frac{\partial v}{\partial y}\right) + \frac{\partial}{\partial z}\mu\left(\frac{\partial v}{\partial z} + \frac{\partial w}{\partial y}\right) + Y\rho \quad (18)$$

$$\rho\frac{Dw}{Dt} = -\frac{\partial p}{\partial z} - \frac{2}{3}\frac{\partial}{\partial z}\mu\left(\frac{\partial u}{\partial x} + \frac{\partial v}{\partial y} + \frac{\partial w}{\partial z}\right) + \frac{\partial}{\partial x}\left(\mu\left(\frac{\partial u}{\partial z} + \frac{\partial w}{\partial x}\right)\right) + \frac{\partial}{\partial y}\mu\left(\frac{\partial v}{\partial z} + \frac{\partial w}{\partial y}\right) + 2\frac{\partial}{\partial z}\left(\mu\frac{\partial w}{\partial z}\right) + Z\rho \quad (19)$$

B.2. Continuity Equation

The continuity equation is an expression of conservation of mass, that is, a statement that the total mass entering a control volume minus the total mass total mass exiting the control volume is equal to the accumulation of mass (increase in density) within the control volume.

Beginning with the definition of density, the mass of fluid within the control volume is

$$\rho = \frac{M}{V} \longrightarrow \frac{\partial M}{\partial t} = \frac{\partial \rho}{\partial t}V = \frac{\partial \rho}{\partial t}\partial x\partial y\partial z \quad (20)$$

The time rate of change of mass is then the summation of the net mass flow in each of the three dimensions. Beginning with the x-direction:

$$A_x = \partial y \partial z$$

$$\dot{m}_x = \rho u A_x$$

$$\dot{m}_{x,in} = \left(\rho u - \frac{\partial \rho u}{\partial x} \frac{dx}{2} \right) \partial y \partial z$$

$$\dot{m}_{x,out} = \left(\rho u + \frac{\partial \rho u}{\partial x} \frac{dx}{2} \right) \partial y \partial z$$

$$\dot{m}_{x,in} - \dot{m}_{x,out} = \left(\rho u - \frac{\partial \rho u}{\partial x} \frac{dx}{2} \right) \partial y \partial z - \left(\rho u + \frac{\partial \rho u}{\partial x} \frac{dx}{2} \right) \partial y \partial z$$

$$\dot{m}_{x,net} = -\left(\frac{\partial \rho u}{\partial x} dx \partial y \partial z \right) \tag{21}$$

Mass flow rates in the Y and Z directions are developed in a similar manner resulting in

$$\dot{m}_{y,net} = -\left(\frac{\partial \rho v}{\partial y} dx \partial y \partial z \right) \tag{22}$$

$$\dot{m}_{z,net} = -\left(\frac{\partial \rho w}{\partial z} dx \partial y \partial z \right) \tag{23}$$

and then combining the net mass flows:

$$\frac{dM}{dt} = \frac{\partial \rho}{\partial t} \partial x \partial y \partial z$$

$$\frac{dM}{dt} = \dot{m}_{x,net} + \dot{m}_{y,net} + \dot{m}_{z,net}$$

$$\frac{dM}{dt} = -\left(\frac{\partial \rho u}{\partial x} dx \partial y \partial z \right) - \left(\frac{\partial \rho v}{\partial y} dx \partial y \partial z \right) - \left(\frac{\partial \rho w}{\partial z} dx \partial y \partial z \right) = \frac{\partial \rho}{\partial t} \partial x \partial y \partial z$$

resulting in the continuity equation:

$$\frac{\partial \rho}{\partial t} + \frac{\partial \rho u}{\partial x} + \frac{\partial \rho v}{\partial y} + \frac{\partial \rho w}{\partial z} = 0 \qquad (24)$$

B.3. Thermodynamic Equation of State

For cases involving compressible fluids, the Thermodynamic Equation of State is added to the system of equations to relate pressure, temperature, and density. If an ideal gas is assumed, the characteristic equation is

$$P = \rho RT \qquad (25)$$

where P is the pressure, R is the gas constant, and T is the temperature in Kelvin. Bearing lubrication, however, typically assumes the lubricant is an incompressible fluid.

B.4. Conservation of Energy Equation

Finally, the Conservation of Energy Equation, also known as the First Law of Thermodynamics, is included where the temperature of the fluid is not assumed to be constant (isothermal). The First Law states that the time rate of change of energy stored in a system is equal to the sum of energy added to a system and work performed by the system.

$$\rho C_p \left(\frac{\partial T}{\partial t} + v_\theta \frac{\partial T}{\partial r} + \frac{v_z}{r} \frac{\partial T}{\partial \theta} + v_r \frac{\partial T}{\partial z} \right) = \frac{1}{r} \frac{\partial}{\partial r} \left(kr \frac{\partial T}{\partial r} \right) + \frac{1}{r^2} \frac{\partial}{\partial \theta} \left(k \frac{\partial T}{\partial \theta} \right) + \frac{\partial}{\partial z} \left(k \frac{\partial T}{\partial z} \right) + \Phi \qquad (26)$$

B.5. Reynolds Equation

In 1885, Beauchamp Tower published his experimental results examining oil lubricated journal bearings which demonstrated the existence of hydrodynamic pressure in a bearing's lubricant film. The following year, Osbourne Reynolds published his celebrated analytical paper [6] reviewing and analyzing the results of Tower's experimental results, and in doing so, derived a simplified version of the Navier-Stokes Equations which allowed for the mathematical derivation of pressure gradients in cylindrical journal bearings.

In his derivations, Reynolds began with Stoke's expressions for stress and strain in a fluid and then substitutes their values into the equation of motion and assumed a constant viscosity to arrive at a simplified version of the Navier-Stoke's Equations:

$$\rho\frac{Du}{Dt} = +X\rho - \frac{\partial p}{\partial x} - \frac{2}{3}\frac{\partial}{\partial x}\mu\left(\frac{\partial u}{\partial x} + \frac{\partial v}{\partial y} + \frac{\partial w}{\partial z}\right) + 2\frac{\partial}{\partial x}\left(\mu\frac{\partial u}{\partial x}\right) + \frac{\partial}{\partial y}\left[\mu\left(\frac{\partial u}{\partial y} + \frac{\partial v}{\partial x}\right)\right] + \frac{\partial}{\partial z}\left[\mu\left(\frac{\partial u}{\partial z} + \frac{\partial w}{\partial x}\right)\right]$$

$$\rho\frac{Du}{Dt} = +X\rho - \frac{\partial p}{\partial x} - \frac{2}{3}\frac{\partial}{\partial x}\mu\left(\frac{\partial u}{\partial x} + \frac{\partial v}{\partial y} + \frac{\partial w}{\partial z}\right) + 2\frac{\partial}{\partial x}\left(\mu\frac{\partial u}{\partial x}\right) + \frac{\partial}{\partial y}\left[\mu\left(\frac{\partial u}{\partial y} + \frac{\partial v}{\partial x}\right)\right] + \frac{\partial}{\partial z}\left[\mu\left(\frac{\partial u}{\partial z} + \frac{\partial w}{\partial x}\right)\right]$$

$$\rho\frac{Du}{Dt} = X\rho - \frac{\partial p}{\partial x} + \mu\left(-\frac{2}{3}\frac{\partial}{\partial x}\left(\frac{\partial u}{\partial x} + \frac{\partial v}{\partial y} + \frac{\partial w}{\partial z}\right) + 2\frac{\partial}{\partial x}\left(\frac{\partial u}{\partial x}\right) + \frac{\partial}{\partial y}\left(\frac{\partial u}{\partial y} + \frac{\partial v}{\partial x}\right) + \frac{\partial}{\partial z}\left(\frac{\partial u}{\partial z} + \frac{\partial w}{\partial x}\right)\right)$$

$$\rho\frac{Du}{Dt} = X\rho - \frac{\partial p}{\partial x} + \mu\left(-\frac{2}{3}\frac{\partial}{\partial x}\left(\frac{\partial u}{\partial x} + \frac{\partial v}{\partial y} + \frac{\partial w}{\partial z}\right) + 2\frac{\partial}{\partial x}\left(\frac{\partial u}{\partial x}\right) + \frac{\partial}{\partial y}\left(\frac{\partial u}{\partial y} + \frac{\partial v}{\partial x}\right) + \frac{\partial}{\partial z}\left(\frac{\partial u}{\partial z} + \frac{\partial w}{\partial x}\right)\right)$$

$$\rho\frac{Du}{Dt} = X\rho - \frac{\partial p}{\partial x} + \mu\left(-\frac{2}{3}\frac{\partial^2 u}{\partial x^2} - \frac{2}{3}\frac{\partial^2 v}{\partial x\partial y} - \frac{2}{3}\frac{\partial^2 w}{\partial x\partial z} + 2\frac{\partial^2 u}{\partial x^2} + \frac{\partial^2 u}{\partial y^2} + \frac{\partial^2 v}{\partial x\partial y} + \frac{\partial^2 u}{\partial z^2} + \frac{\partial^2 w}{\partial x\partial z}\right)$$

$$\rho\frac{Du}{Dt} = X\rho - \frac{\partial p}{\partial x} + \mu\left(-\frac{2}{3}\frac{\partial^2 u}{\partial x^2} + 2\frac{\partial^2 u}{\partial x^2} + \frac{\partial^2 u}{\partial y^2} + \frac{\partial^2 u}{\partial z^2} - \frac{2}{3}\frac{\partial^2 v}{\partial x\partial y} + \frac{\partial^2 v}{\partial x\partial y} - \frac{2}{3}\frac{\partial^2 w}{\partial x\partial z} + \frac{\partial^2 w}{\partial x\partial z}\right)$$

$$\rho\frac{Du}{Dt} = X\rho - \frac{\partial p}{\partial x} + \mu\left(\frac{1}{3}\frac{\partial^2 u}{\partial x^2} + \frac{\partial^2 u}{\partial x^2} + \frac{\partial^2 u}{\partial y^2} + \frac{\partial^2 u}{\partial z^2} + \frac{1}{3}\frac{\partial^2 v}{\partial x\partial y} + \frac{1}{3}\frac{\partial^2 w}{\partial x\partial z}\right)$$

$$\rho\frac{Du}{Dt} = X\rho - \frac{\partial p}{\partial x} + \mu\left(\frac{\partial^2 u}{\partial x^2} + \frac{\partial^2 u}{\partial y^2} + \frac{\partial^2 u}{\partial z^2}\right) + \mu\left(\frac{1}{3}\frac{\partial^2 u}{\partial x^2} + \frac{1}{3}\frac{\partial^2 v}{\partial x\partial y} + \frac{1}{3}\frac{\partial^2 w}{\partial x\partial z}\right)$$

$$\rho\frac{Du}{Dt} = X\rho - \frac{\partial p}{\partial x} + \mu\left(\frac{\partial^2 u}{\partial x^2} + \frac{\partial^2 u}{\partial y^2} + \frac{\partial^2 u}{\partial z^2}\right) + \frac{\mu}{3}\left(\frac{\partial^2 u}{\partial x^2} + \frac{\partial^2 v}{\partial x\partial y} + \frac{\partial^2 w}{\partial x\partial z}\right)$$

$$\rho\frac{Du}{Dt} = X\rho - \frac{\partial p}{\partial x} + \mu\left(\frac{\partial^2 u}{\partial x^2} + \frac{\partial^2 u}{\partial y^2} + \frac{\partial^2 u}{\partial z^2}\right) + \frac{\mu}{3}\frac{\partial}{\partial x}\left(\frac{\partial u}{\partial x} + \frac{\partial v}{\partial y} + \frac{\partial w}{\partial z}\right) \qquad (27)$$

In his derivations, Reynolds employed the Navier-Stokes equations in Cartesian coordinates vice a cylindrical coordinate system. This is based on the radii of curvature of the

fluid film compared to the thickness of the film, allowing the curvature to be disregarded and therefore treated as a case of parallel plates.

Reynolds then notes that the depth of the fluid film is very small such that the fluid is free from eddies and that the weight and that the inertial forces are small compared to the stressed arising from viscosity. He also notes that the effects of inertial and body forces are small in comparison to the effect of viscous terms allowing the inertial and body force terms to be omitted. Finally, he also notes that oils very closely approximate an incompressible fluid allowing for the omission of the dilation term:

$$\rho(0) = (0)\rho - \frac{\partial p}{\partial x} + \mu\left(\frac{\partial^2 u}{\partial x^2} + \frac{\partial^2 u}{\partial y^2} + \frac{\partial^2 u}{\partial z^2}\right) + \frac{\mu}{3}\frac{\partial}{\partial x}(0) \qquad (28)$$

Upon rearranging, including similar derivations in the y and z directions, and including the continuity equation (eq (24)) simplified for an incompressible fluid, results in:

$$\frac{\partial p}{\partial x} = \mu\left(\frac{\partial^2 u}{\partial x^2} + \frac{\partial^2 u}{\partial y^2} + \frac{\partial^2 u}{\partial z^2}\right) \qquad (29)$$

$$\frac{\partial p}{\partial y} = \mu\left(\frac{\partial^2 v}{\partial x^2} + \frac{\partial^2 v}{\partial y^2} + \frac{\partial^2 v}{\partial z^2}\right) \qquad (30)$$

$$\frac{\partial p}{\partial z} = \mu\left(\frac{\partial^2 w}{\partial x^2} + \frac{\partial^2 w}{\partial y^2} + \frac{\partial^2 w}{\partial z^2}\right) \qquad (31)$$

$$0 = \frac{\partial u}{\partial x} + \frac{\partial v}{\partial y} + \frac{\partial w}{\partial z} \qquad (32)$$

Reynolds then aligned with x-dimension with the direction of relative motion of the bearing, the z-dimension along the axis of the bearing, and the y-dimension perpendicular to the surface of the bearing. He then noted that the y-component of the velocity of fluid (v) would be small compared to the x and z components, u and w, respectively. Finally, he theorized that variations in u and w would be small compared to variations in v:

$$\frac{\partial p}{\partial x} = \mu \frac{\partial^2 u}{\partial y^2} \qquad (33)$$

$$\frac{\partial p}{\partial y} = 0 \qquad (34)$$

$$\frac{\partial p}{\partial z} = \mu \frac{\partial^2 w}{\partial y^2} \qquad (35)$$

$$0 = \frac{\partial u}{\partial x} + \frac{\partial v}{\partial y} + \frac{\partial w}{\partial z} \qquad (36)$$

Assuming that pressure (p) and viscosity (μ) are independent of y, eq (33) may be integrated directly:

$$\frac{\partial p}{\partial x} = \mu \frac{\partial^2 u}{\partial y^2}$$

$$\frac{\partial^2 u}{\partial y^2} = \frac{1}{\mu}\frac{\partial p}{\partial x}$$

$$\int \frac{\partial^2 u}{\partial y^2} dy = \int \frac{1}{\mu}\frac{\partial p}{\partial x} dy$$

$$\frac{\partial u}{\partial y} = \frac{y}{\mu}\frac{\partial p}{\partial x} + A$$

$$\int \frac{\partial u}{\partial y} dy = \int \left(\frac{1}{\mu}\frac{\partial py}{\partial x} + A \right) dy$$

$$u = \frac{y^2}{2\mu}\frac{\partial p}{\partial x} + Ay + B \qquad (37)$$

and similarly for eq (35):

$$w = \frac{w^2}{2\mu}\frac{\partial p}{\partial x} + Cw + D \qquad (38)$$

It is important to note that the viscosity will rarely be constant across the fluid film (y direction) as is assumed here; in reality, temperature variations across the film have the potential to result in considerable variation in the viscosity. However, assuming an average viscosity is satisfactory in most applications and results in a substantially simpler derivation.

Boundary conditions are then considered in order to evaluate the constants of integration, A, B, C, and D. Reynolds assumed that the velocity of the fluid at the wetted surface (u) is equal to the velocity of the wetted surface itself (U), that there is no axial sliding motion (z dimension) and that the pressure of the fluid film at the film's extremities is dependent upon external conditions. Considering y at the journal surface to equal 0 and h at the bearing surface results in:

$$\text{At y} = 0 \begin{cases} u_{y=0} = U_0 \\ v_{y=0} = 0 \\ w_{y=0} = 0 \end{cases} \qquad \text{At y} = \text{h} \begin{cases} u_{y=h} = U_1 \\ v_{y=h} = U_1 \dfrac{dh}{dx} + V \\ w_{y=h} = 0 \end{cases} \qquad f(xy) = 0 \qquad p = p_0$$

The constant of integration B in eq (37) may then be determined at Y = 0:

$$\begin{aligned} u &= \frac{y^2}{2\mu}\frac{\partial p}{\partial x} + Ay + B \\ U_0 &= B \end{aligned} \qquad (39)$$

and the constant of integration A in eq (37) may be determined at Y = h:

$$\begin{aligned} u &= \frac{y^2}{2\mu}\frac{\partial p}{\partial x} + Ay + B \\ U_1 &= \frac{h^2}{2\mu}\frac{\partial p}{\partial x} + Ah + U_0 \\ A &= \frac{U_1 - U_0}{h} - \frac{h}{2\mu}\frac{\partial p}{\partial x} \end{aligned} \qquad (40)$$

Substituting these back into equation eq (37) and simplifying results in:

$$\begin{aligned} u &= \frac{y^2}{2\mu}\frac{\partial p}{\partial x} + \left(\frac{U_1 - U_0}{h} - \frac{h}{2\mu}\frac{\partial p}{\partial x}\right)y + U_0 \\ u &= \underbrace{\left(y^2 - yh\right)\frac{\partial p}{2\mu\partial x}}_{\text{Poiseuille Flow Term}} + \underbrace{\frac{y}{h}\left(U_1 - U_0\right) + U_0}_{\text{Couette Flow Term}} \end{aligned} \qquad (41)$$

The Poiseuille Flow Term, named after the French Physician who studied the flow of human blood, represents the flow induced as a result of the pressure gradient. The Couette Flow Term, named after the French Physicist best known for his work with viscous fluids, represents the velocity effects on the fluid flow.

The rate of fluid flow in the x direction, q_x, may then be determined:

$$u = \left(y^2 - yh\right)\frac{\partial p}{2\mu\partial x} + \frac{y}{h}\left(U_1 - U_0\right) + U_0$$

$$q_x = \int_0^h u dy$$

$$q_x = \left(\frac{y^3}{3} - \frac{y^2 h}{2}\right)\frac{\partial p}{2\mu\partial x}\bigg|_0^h + \frac{y^2}{2h}\left(U_1 - U_0\right)\bigg|_0^h + U_0 y\big|_0^h$$

$$q_x = -\frac{h^3}{12}\frac{\partial p}{\mu\partial x} + \frac{h}{2}\left(U_1 + U_0\right) \qquad (42)$$

Following an identical process, the flow in the z direction may be found:

$$q_z = -\frac{h^3}{12}\frac{\partial p}{\mu\partial x} + \frac{h}{2}\left(W_1 + W_0\right) \qquad (43)$$

where V_1 and V_0 are the axial velocities of the bearing and journal respectively.

Further derivation requires a returning to the concept of the Continuity Equation (eq (24)) as discussed in section B.2. However, this derivation, which relies heavily on the derivation presented by Cameron [5], is based on the assumption of steady-state, incompressible flow and a control volume bounded on the top and bottom by the bearing and journal surfaces respectively. The control volume assumed has a base with an area of dxdz and a height of h, the film thickness.

The resulting rate of flow into the control volume in the X and Z dimensions would be:

$$q_x dz - \left(q_x + \frac{\partial q_x}{\partial x} dx \right) dz$$
$$q_z dx - \left(q_z + \frac{\partial q_z}{\partial z} dz \right) dx \qquad (44)$$

and the total inflow is then

$$-\left(\frac{\partial q_x}{\partial x} + \frac{\partial q_z}{\partial z} \right) dxdz \qquad (45)$$

As noted above, the control volume is bounded on the top and bottom by the bearing and journal surfaces respectively. If the base (the journal) moves with a velocity of V_0 or the top (the bearing) moves with a velocity V_1, a change in the volume of fluid (dxdydz) element results where dy is equal to $V_1 - V_0$. This change in volume may then be equated to a fluid flow because a fluid flowing into our out of the control volume in the y direction would have the same effect on the volume of the fluid element. The total inflow becomes:

$$\left(V_1 - V_0 \right) dxdz = -\left(\frac{\partial q_x}{\partial x} + \frac{\partial q_z}{\partial z} \right) dxdz$$
$$\frac{\partial q_x}{\partial x} + \left(V_1 - V_0 \right) + \frac{\partial q_z}{\partial z} = 0 \qquad (46)$$

By then entering the flow terms shown in eq (42) and eq (43) into this simplified version of the continuity equation the Reynolds Equation for an incompressible fluid with constant viscosity may be found:

$$\frac{\partial}{\partial x}\left(-\frac{h^3}{12}\frac{\partial p}{\mu\partial x}+\frac{h}{2}\left(U_1+U_0\right)\right)+\left(V_1-V_0\right)+\frac{\partial}{\partial z}\left(-\frac{h^3}{12}\frac{\partial p}{\mu\partial x}+\frac{h}{2}\left(W_1+W_0\right)\right)=0 \qquad (47)$$

$$\frac{\partial}{\partial x}\left(\frac{h^3}{\mu}\frac{\partial p}{\partial x}\right)+\frac{\partial}{\partial z}\left(\frac{h^3}{\mu}\frac{\partial p}{\partial x}\right)=6\left(h\left(U_1+U_0\right)\frac{\partial}{\partial x}+2\left(V_1-V_0\right)+h\left(W_1+W_0\right)\frac{\partial}{\partial z}\right) \qquad (48)$$